AD-A074 517 NAVAL OCEAN SYSTEMS CENTER SAN DIEGO CA F/G 9/1
SPECTRAL, FAR-FIELD, AND NEAR-FIELD MEASUREMENTS OF FIVE LIGHT---ETC(U)
JUL 79 C R ZEISSE, S A MILLER
UNCLASSIFIED NOSC-TD-265 NL

| OF |
AD
A074517

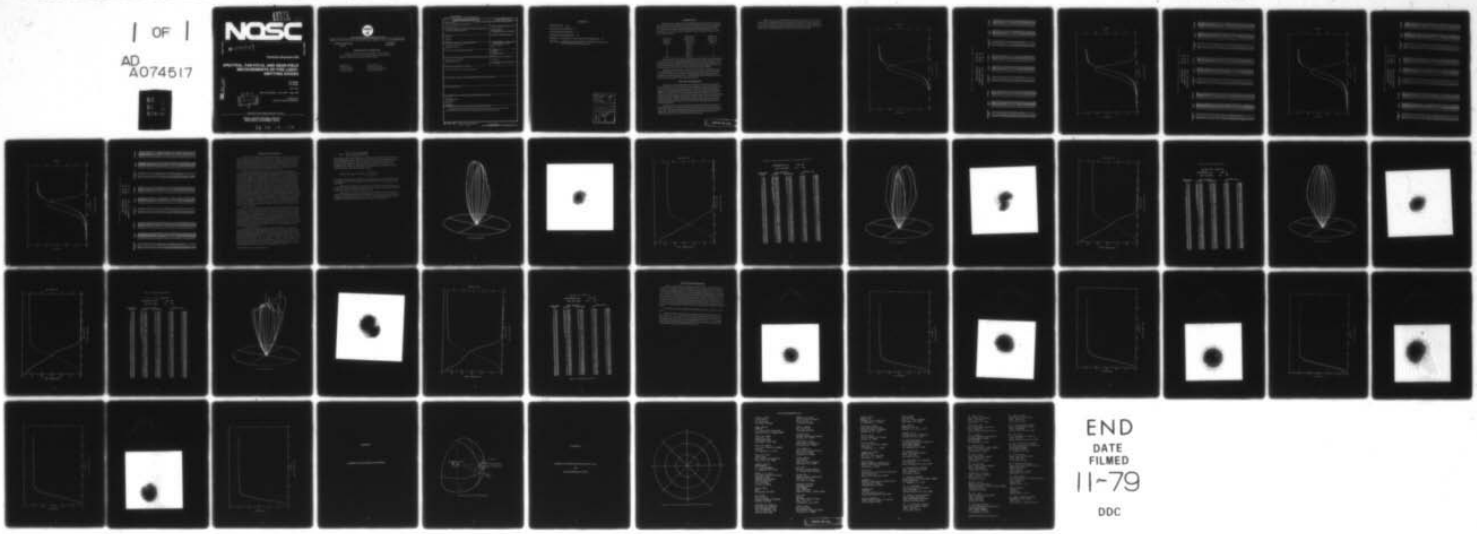

END
DATE
FILMED
11-79
DDC

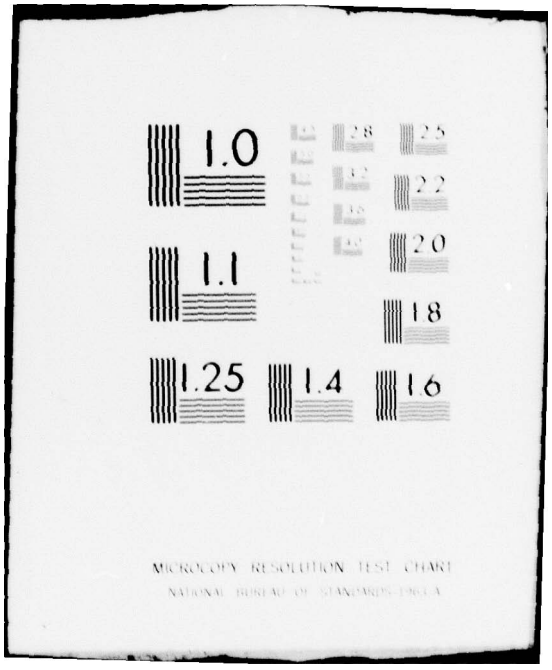
1.0
1.1
1.25
1.4
1.6
2.8
2.5
2.2
2.0
1.8
MICROCOPY RESOLUTION TEST CHART
NATIONAL BUREAU OF STANDARDS 1963-A

NOSC

NOSC TD 265

Technical Document 265

SPECTRAL, FAR-FIELD, AND NEAR-FIELD MEASUREMENTS OF FIVE LIGHT-EMITTING DIODES

CR Zeisse
SA Miller

JULY 1979

Test and Evaluation: April 1979 — May 1979

Prepared for
Naval Air Systems Command

Approved for public release; distribution unlimited

NAVAL OCEAN SYSTEMS CENTER
SAN DIEGO, CALIFORNIA 92152

NAVAL OCEAN SYSTEMS CENTER, SAN DIEGO, CA 92152

AN ACTIVITY OF THE NAVAL MATERIAL COMMAND

SL GUILLE, CAPT, USN
Commander

HL BLOOD
Technical Director

ADMINISTRATIVE INFORMATION

Work was performed during April and May 1979 under NOSC 63728N, Z1050-SL, ET-15 by the Electronic Material Sciences Division. Work was sponsored by Naval Air Systems Command.

Released by
HH Wieder, Head
Electronic Material
Sciences Division

Under Authority of
CD Pierson, Jr., Head
Electronic Engineering and
Sciences Department

UNCLASSIFIED

SECURITY CLASSIFICATION OF THIS PAGE (When Data Entered)

REPORT DOCUMENTATION PAGE

READ INSTRUCTIONS BEFORE COMPLETING FORM

1. REPORT NUMBER: NOSC Technical Document 265 (TD 265)	2. GOVT ACCESSION NO.
3. RECIPIENT'S CATALOG NUMBER	
4. TITLE (and Subtitle): SPECTRAL, FAR-FIELD, AND NEAR-FIELD MEASUREMENTS OF FIVE LIGHT-EMITTING DIODES	5. TYPE OF REPORT & PERIOD COVERED: Test and evaluation, April – May 1979
	6. PERFORMING ORG. REPORT NUMBER
7. AUTHOR(s): CR Zeisse, SA Miller	8. CONTRACT OR GRANT NUMBER(s)
9. PERFORMING ORGANIZATION NAME AND ADDRESS: Naval Ocean Systems Center, San Diego, CA 92152	10. PROGRAM ELEMENT, PROJECT, TASK AREA & WORK UNIT NUMBERS: 63728N, Z1050-SL, ET-15
11. CONTROLLING OFFICE NAME AND ADDRESS	12. REPORT DATE: July 1979
	13. NUMBER OF PAGES: 45
14. MONITORING AGENCY NAME & ADDRESS (if different from Controlling Office): Naval Air Systems Command, Washington, DC 20361	15. SECURITY CLASS. (of this report): Unclassified
	15a. DECLASSIFICATION/DOWNGRADING SCHEDULE

16. DISTRIBUTION STATEMENT (of this Report)

Approved for public release; distribution unlimited.

17. DISTRIBUTION STATEMENT (of the abstract entered in Block 20, if different from Report)

18. SUPPLEMENTARY NOTES

19. KEY WORDS (Continue on reverse side if necessary and identify by block number)

Far field
Light emitting diodes
Measurement
Near field
Spectrometry

20. ABSTRACT (Continue on reverse side if necessary and identify by block number)

The report presents results of near-field, spectral, and far-field measurements performed on 5 light emitting diodes selected at random from 45 manufactured by Laser Diode Laboratories.

DD FORM 1 JAN 73 1473 EDITION OF 1 NOV 65 IS OBSOLETE
S/N 0102-LF-014-6601

UNCLASSIFIED

SECURITY CLASSIFICATION OF THIS PAGE (When Data Entered)

CONTENTS :

INTRODUCTION

During the week of April 16, 1979, 45 light-emitting diodes (LEDs) were received at the Naval Ocean Systems Center (NOSC) from Laser Diode Laboratories, Incorporated. These diodes were produced under manufacturing technology contract number N00123-78-C-05700 for the purpose of improving LEDs for fiber bundle applications. Out of the diodes received, 5 were selected at random for further evaluation and assigned device serial numbers as follows:

Laser Diode Laboratory Number	Naval Ocean Systems Center Device Serial Number	Notation for Figures and Tables in this Report
5	DSN118	a
15	DSN119	b
25	DSN120	c
36	DSN121	d
40	DSN122	e

Near-field, spectral, and far-field measurements (in that order) were then performed on each of the 5 diodes. A thin aperture, 0.045 inch in diameter, was centered on the face of each diode for the far-field and near-field measurements. During the beginning of the spectral measurement for DSN121, the diode open-circuited while 100 mA of current was flowing through it. Hence only near-field measurements appear for DSN121.

The purpose of this report is to present the results of these measurements, which were completed May 24, 1979. The measurements are presented in the following order: (1) spectral, (2) far-field, (3) near-field. A brief paragraph describing the measurement method and purpose begins each section. To facilitate the visual presentation of the data, the figures are not presented in the usual numerical order.

SPECTRAL MEASUREMENTS

The purpose of these measurements is to determine the relative spectral radiant power of the LED. To do this, the diode is driven with direct current and the radiant flux is focused with mirrors onto the entrance slit of a Jarrell-Ash 0.5-meter grating monochromator. The monochromatic light leaving the exit slit is focused onto an RCA model 30809 silicon photodetector. The optical beam is chopped at 20 Hz by a mechanical chopper in front of the entrance slit, and the resulting ac signal in the detector is amplified, rectified by a lock-in, digitized, and stored in computer memory as the raw data file for that particular diode. The raw data file is then corrected to take into account spectral variations not associated with the source and to adjust the wavelength marker from its nominal to true value.

Figures 1(a), (b), (c), and (e) show the relative spectral radiant flux $\Lambda(\lambda)$ and its integral with respect to wavelength for all diodes except (d), the one that developed an open circuit. The flux has been normalized so that its integral with respect to wavelength equals unity. Each diode was operated at 100 mA dc and the optical resolution was always better than 0.13 nm. Data were taken at 2-nm intervals.

Tables 1(a), (b), (c) and (e) present the data of figures 1(a), (b), (c), (d) in tabular form. The peak wavelength is the wavelength at which the spectral flux is a maximum. The average wavelength separates the spectrum into two equal areas: half the total flux lies at shorter wavelengths, and half the total flux lies at longer wavelengths. The spectral width is defined as the full width of the peak at half of its maximum value.

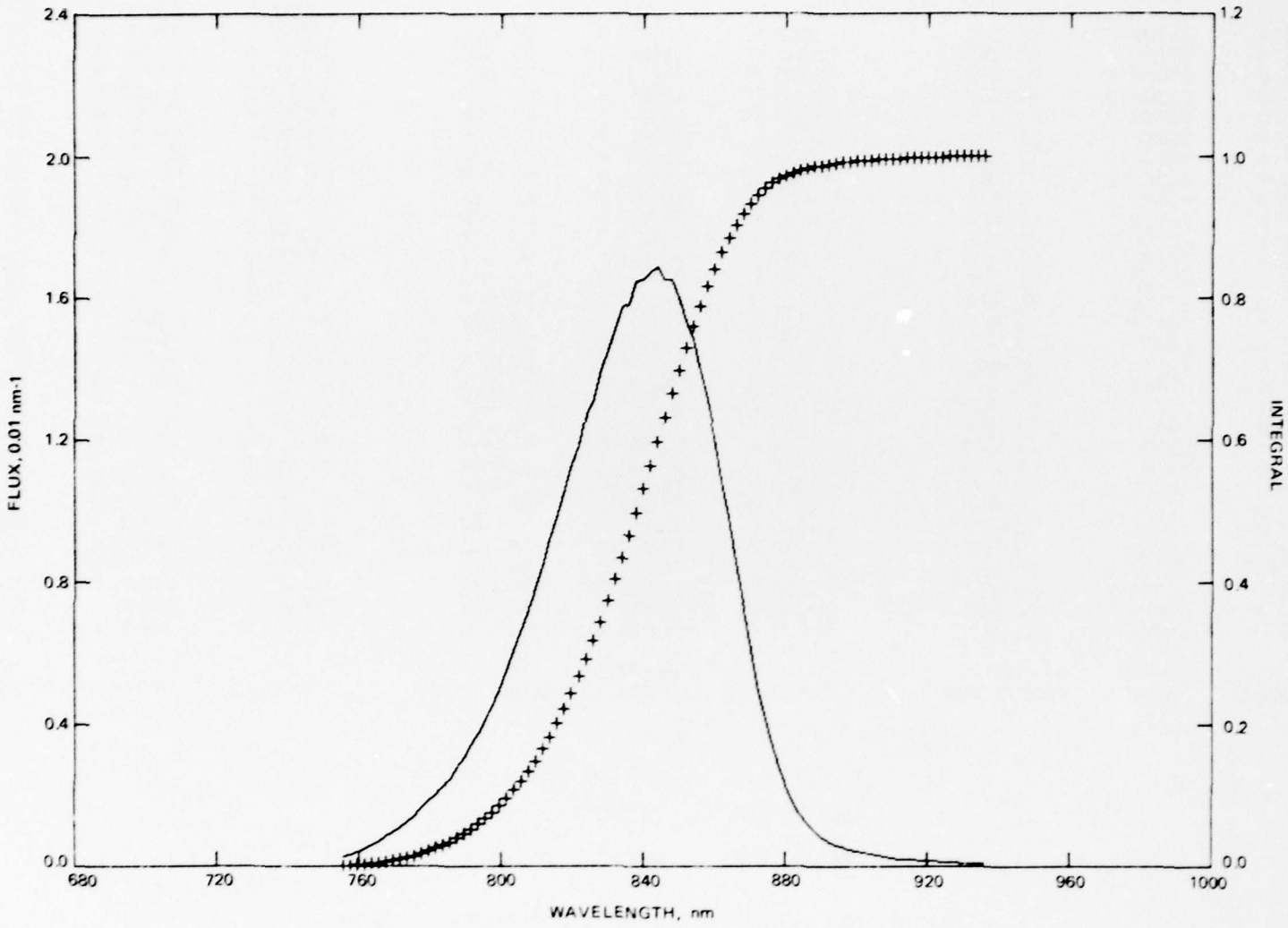

Figure 1(a). DSN118.S00.

Table 1(a). Relative spectral flux. Raw data file: DSN118.S00.

PEAK WAVELENGTH: 844.00 NM

AVERAGE WAVELENGTH: 838.08 NM

SPECTRAL WIDTH (FWHM): 54.38 NM

WAVELENGTH (NM)	FLUX (NM-1)	INTEGRAL	WAVELENGTH (NM)	FLUX (NM-1)	INTEGRAL	WAVELENGTH (NM)	FLUX (NM-1)	INTEGRAL
755.79	0.00026	0.00000	757.79	0.00034	0.00060	759.79	0.00042	0.00135
761.79	0.00048	0.00225	763.79	0.00062	0.00335	765.79	0.00068	0.00464
767.79	0.00084	0.00616	769.80	0.00094	0.00794	771.80	0.00108	0.00997
773.81	0.00124	0.01231	775.81	0.00142	0.01497	777.82	0.00162	0.01802
779.82	0.00183	0.02146	781.82	0.00202	0.02531	783.83	0.00223	0.02958
785.83	0.00250	0.03431	787.84	0.00278	0.03962	789.84	0.00307	0.04547
791.85	0.00343	0.05200	793.85	0.00375	0.05918	795.86	0.00412	0.06709
797.86	0.00453	0.07575	799.87	0.00501	0.08534	801.87	0.00551	0.09586
803.88	0.00607	0.10749	805.88	0.00659	0.12015	807.89	0.00710	0.13391
809.90	0.00785	0.14893	811.90	0.00844	0.16521	813.91	0.00919	0.18292
815.91	0.00979	0.20190	817.92	0.01050	0.22229	819.92	0.01122	0.24401
821.93	0.01185	0.26718	823.93	0.01270	0.29173	825.94	0.01316	0.31772
827.95	0.01395	0.34497	829.95	0.01452	0.37343	831.96	0.01512	0.40322
833.96	0.01572	0.43406	835.97	0.01586	0.46580	837.98	0.01649	0.49830
839.98	0.01651	0.53131	841.99	0.01672	0.56471	844.00	0.01687	0.59847
846.00	0.01653	0.63186	848.01	0.01651	0.66507	850.01	0.01600	0.69758
852.02	0.01536	0.72911	854.02	0.01486	0.75933	856.02	0.01390	0.78809
858.03	0.01313	0.81526	860.03	0.01208	0.84047	862.03	0.01083	0.86338
864.04	0.00984	0.88416	866.04	0.00857	0.90257	868.05	0.00742	0.91864
870.05	0.00632	0.93238	872.05	0.00514	0.94385	874.06	0.00427	0.95330
876.06	0.00353	0.96110	878.07	0.00285	0.96751	880.07	0.00230	0.97266
882.08	0.00184	0.97682	884.08	0.00148	0.98013	886.09	0.00124	0.98286
888.09	0.00103	0.98513	890.10	0.00084	0.98700	892.10	0.00072	0.98856
894.10	0.00061	0.98988	896.11	0.00055	0.99105	898.11	0.00045	0.99209
900.11	0.00043	0.99302	902.12	0.00039	0.99384	904.12	0.00035	0.99458
906.13	0.00031	0.99526	908.13	0.00029	0.99586	910.13	0.00024	0.99639
912.14	0.00021	0.99685	914.14	0.00019	0.99726	916.14	0.00018	0.99764
918.14	0.00017	0.99799	920.15	0.00016	0.99832	922.15	0.00014	0.99862
924.15	0.00013	0.99889	926.15	0.00011	0.99913	928.15	0.00010	0.99934
930.15	0.00009	0.99954	932.15	0.00007	0.99971	934.15	0.00007	0.99985
936.15	0.00007	1.00000						

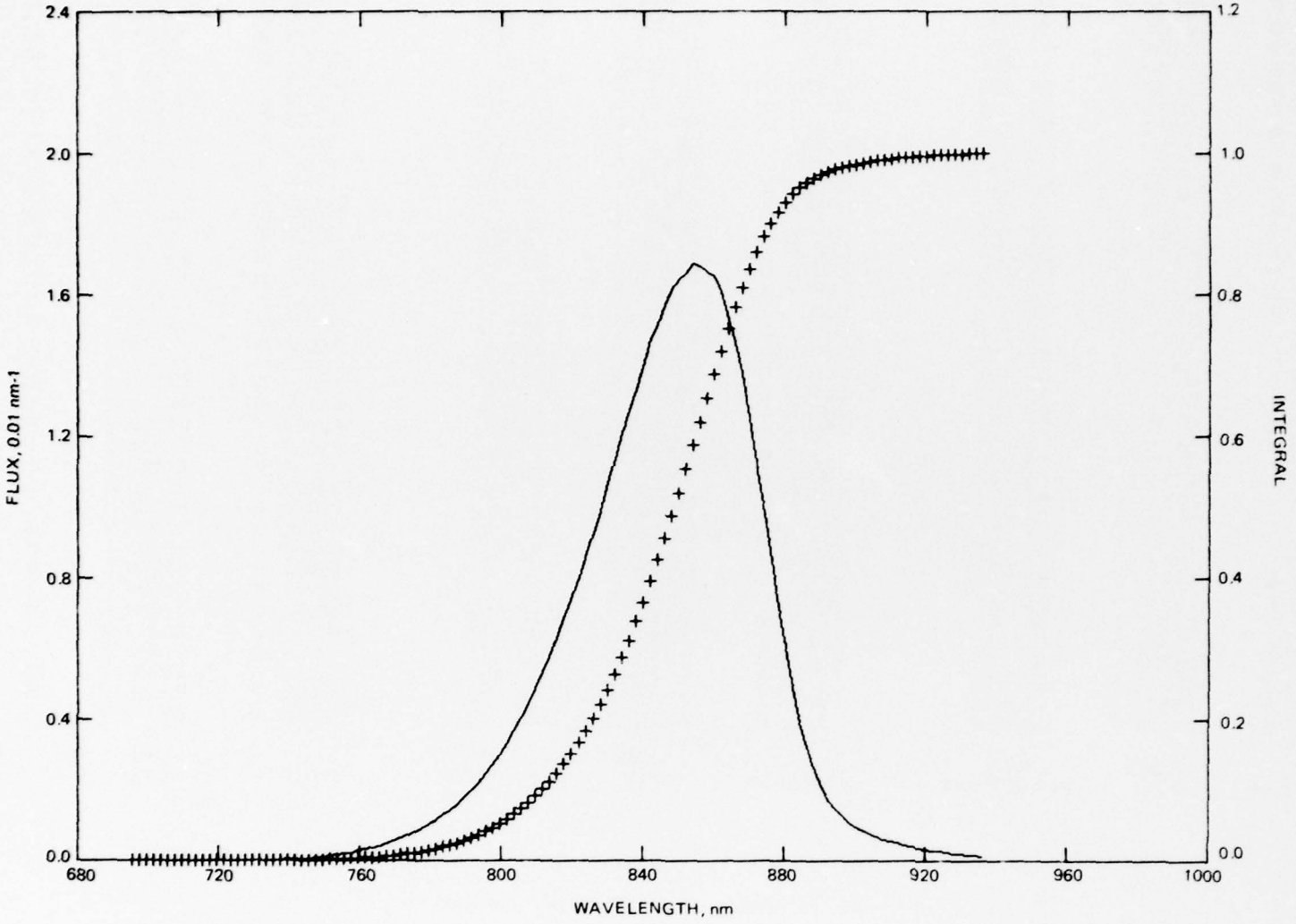

Figure 1(b). DSN119.S00.

Table 1(b). Relative spectral flux. Raw data file: DSN119.S00.

PEAK WAVELENGTH: 854.02 NM

AVERAGE WAVELENGTH: 848.74 NM

SPECTRAL WIDTH (FWHM): 53.44 NM

WAVELENGTH (NM)	FLUX (NM-1)	INTEGRAL	WAVELENGTH (NM)	FLUX (NM-1)	INTEGRAL	WAVELENGTH (NM)	FLUX (NM-1)	INTEGRAL
695.79	0.00002	0.00000	697.79	0.00000	0.00002	699.79	0.00002	0.00003
701.79	0.00002	0.00007	703.79	0.00000	0.00009	705.79	0.00001	0.00010
707.79	0.00001	0.00012	709.79	0.00001	0.00014	711.79	0.00000	0.00015
713.79	0.00001	0.00017	715.79	0.00000	0.00018	717.79	0.00001	0.00020
719.79	0.00001	0.00022	721.79	0.00001	0.00025	723.79	0.00001	0.00027
725.79	0.00001	0.00029	727.79	0.00001	0.00032	729.79	0.00001	0.00034
731.79	0.00001	0.00035	733.79	0.00002	0.00038	735.79	0.00001	0.00041
737.79	0.00002	0.00044	739.79	0.00003	0.00048	741.79	0.00002	0.00053
743.79	0.00004	0.00060	745.79	0.00005	0.00069	747.79	0.00007	0.00081
749.79	0.00009	0.00097	751.79	0.00011	0.00117	753.79	0.00015	0.00143
755.79	0.00018	0.00177	757.79	0.00021	0.00216	759.79	0.00027	0.00263
761.79	0.00032	0.00322	763.79	0.00037	0.00391	765.79	0.00042	0.00470
767.79	0.00048	0.00560	769.80	0.00056	0.00665	771.80	0.00065	0.00785
773.81	0.00072	0.00923	775.81	0.00082	0.01077	777.82	0.00092	0.01253
779.82	0.00104	0.01449	781.82	0.00116	0.01669	783.83	0.00130	0.01917
785.83	0.00145	0.02193	787.84	0.00160	0.02499	789.84	0.00181	0.02840
791.85	0.00201	0.03223	793.85	0.00222	0.03646	795.86	0.00246	0.04117
797.86	0.00270	0.04633	799.87	0.00302	0.05208	801.87	0.00334	0.05844
803.88	0.00369	0.06550	805.88	0.00403	0.07322	807.89	0.00442	0.08171
809.90	0.00487	0.09105	811.90	0.00534	0.10127	813.91	0.00582	0.11248
815.91	0.00632	0.12462	817.92	0.00687	0.13788	819.92	0.00740	0.15216
821.93	0.00803	0.16767	823.93	0.00872	0.18442	825.94	0.00928	0.20250
827.95	0.00990	0.22177	829.95	0.01069	0.24236	831.96	0.01137	0.26452
833.96	0.01207	0.28796	835.97	0.01274	0.31289	837.98	0.01330	0.33906
839.98	0.01395	0.36631	841.99	0.01472	0.39512	844.00	0.01516	0.42515
846.00	0.01569	0.45600	848.01	0.01617	0.48802	850.01	0.01646	0.52065
852.02	0.01660	0.55387	854.02	0.01687	0.58735	856.02	0.01678	0.62100
858.03	0.01662	0.65458	860.03	0.01653	0.68773	862.03	0.01607	0.72033
864.04	0.01530	0.75185	866.04	0.01463	0.78178	868.05	0.01381	0.81036
870.05	0.01252	0.83669	872.05	0.01125	0.86046	874.06	0.01006	0.88189
876.06	0.00875	0.90070	878.07	0.00745	0.91698	880.07	0.00627	0.93070
882.08	0.00511	0.94213	884.08	0.00409	0.95133	886.09	0.00335	0.95880
888.09	0.00277	0.96492	890.10	0.00222	0.96994	892.10	0.00181	0.97398
894.10	0.00153	0.97731	896.11	0.00131	0.98016	898.11	0.00112	0.98259
900.11	0.00097	0.98467	902.12	0.00086	0.98651	904.12	0.00076	0.98814
906.13	0.00068	0.98959	908.13	0.00062	0.99089	910.13	0.00056	0.99207
912.14	0.00050	0.99313	914.14	0.00045	0.99407	916.14	0.00041	0.99493
918.14	0.00037	0.99570	920.15	0.00033	0.99641	922.15	0.00030	0.99704
924.15	0.00027	0.99760	926.15	0.00024	0.99811	928.15	0.00021	0.99857
930.15	0.00019	0.99898	932.15	0.00017	0.99934	934.15	0.00016	0.99967
936.15	0.00014	0.99997						

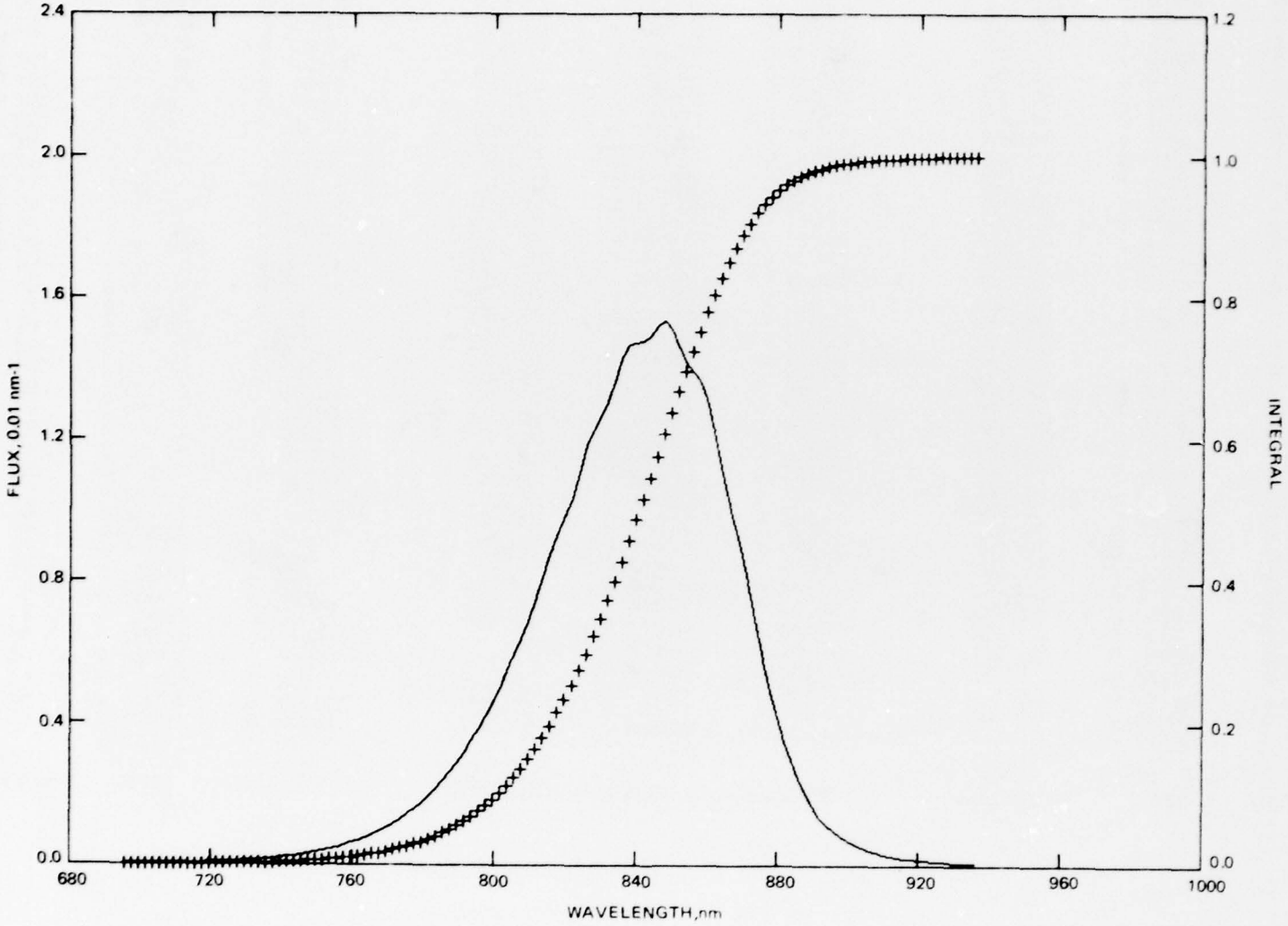

Figure 1(c). DSN120.S00.

Table 1(c). Relative spectral flux. Raw data file: DSN120.S00.

PEAK WAVELENGTH: 848.01 NM

AVERAGE WAVELENGTH: 840.86 NM

SPECTRAL WIDTH (FWHM): 59.72 NM

WAVELENGTH (NM)	FLUX (NM-1)	INTEGRAL	WAVELENGTH (NM)	FLUX (NM-1)	INTEGRAL	WAVELENGTH (NM)	FLUX (NM-1)	INTEGRAL
695.79	0.00002	0.00000	697.79	0.00003	0.00005	699.79	0.00003	0.00011
701.79	0.00003	0.00018	703.79	0.00004	0.00025	705.79	0.00004	0.00033
707.79	0.00004	0.00041	709.79	0.00004	0.00049	711.79	0.00005	0.00058
713.79	0.00004	0.00067	715.79	0.00005	0.00076	717.79	0.00006	0.00087
719.79	0.00006	0.00099	721.79	0.00008	0.00113	723.79	0.00009	0.00129
725.79	0.00009	0.00147	727.79	0.00010	0.00166	729.79	0.00011	0.00187
731.79	0.00012	0.00209	733.79	0.00014	0.00235	735.79	0.00015	0.00263
737.79	0.00018	0.00296	739.79	0.00020	0.00333	741.79	0.00023	0.00376
743.79	0.00025	0.00423	745.79	0.00028	0.00477	747.79	0.00031	0.00536
749.79	0.00035	0.00601	751.79	0.00039	0.00675	753.79	0.00044	0.00758
755.79	0.00048	0.00850	757.79	0.00055	0.00953	759.79	0.00062	0.01070
761.79	0.00070	0.01202	763.79	0.00077	0.01349	765.79	0.00085	0.01512
767.79	0.00095	0.01692	769.80	0.00105	0.01893	771.80	0.00116	0.02114
773.81	0.00129	0.02360	775.81	0.00144	0.02632	777.82	0.00160	0.02938
779.82	0.00177	0.03276	781.82	0.00196	0.03648	783.83	0.00217	0.04062
785.83	0.00241	0.04520	787.84	0.00264	0.05028	789.84	0.00289	0.05580
791.85	0.00317	0.06190	793.85	0.00351	0.06859	795.86	0.00386	0.07599
797.86	0.00419	0.08404	799.87	0.00455	0.09283	801.87	0.00497	0.10235
803.88	0.00548	0.11286	805.88	0.00595	0.12430	807.89	0.00638	0.13670
809.90	0.00689	0.15004	811.90	0.00745	0.16437	813.91	0.00813	0.18003
815.91	0.00878	0.19694	817.92	0.00926	0.21507	819.92	0.00975	0.23408
821.93	0.01036	0.25430	823.93	0.01140	0.27576	825.94	0.01182	0.29879
827.95	0.01228	0.32301	829.95	0.01264	0.34793	831.96	0.01308	0.37378
833.96	0.01365	0.40051	835.97	0.01427	0.42857	837.98	0.01468	0.45767
839.98	0.01472	0.48707	841.99	0.01478	0.51672	844.00	0.01494	0.54659
846.00	0.01520	0.57673	848.01	0.01535	0.60744	850.01	0.01513	0.63791
852.02	0.01459	0.66779	854.02	0.01419	0.69658	856.02	0.01393	0.72470
858.03	0.01367	0.75243	860.03	0.01315	0.77926	862.03	0.01224	0.80466
864.04	0.01124	0.82326	866.04	0.01033	0.84982	868.05	0.00957	0.86982
870.05	0.00874	0.88812	872.05	0.00779	0.90466	874.06	0.00677	0.91930
876.06	0.00579	0.93186	878.07	0.00494	0.94264	880.07	0.00418	0.95176
882.08	0.00354	0.95952	884.08	0.00299	0.96605	886.09	0.00248	0.97155
888.09	0.00204	0.97608	890.10	0.00167	0.97981	892.10	0.00137	0.98285
894.10	0.00116	0.98538	896.11	0.00100	0.98756	898.11	0.00085	0.98941
900.11	0.00071	0.99096	902.12	0.00059	0.99226	904.12	0.00050	0.99335
906.13	0.00044	0.99430	908.13	0.00038	0.99512	910.13	0.00033	0.99584
912.14	0.00029	0.99646	914.14	0.00025	0.99700	916.14	0.00022	0.99746
918.14	0.00019	0.99787	920.15	0.00017	0.99823	922.15	0.00015	0.99855
924.15	0.00014	0.99884	926.15	0.00012	0.99910	928.15	0.00011	0.99933
930.15	0.00009	0.99953	932.15	0.00008	0.99971	934.15	0.00007	0.99986
936.15	0.00007	1.00000						

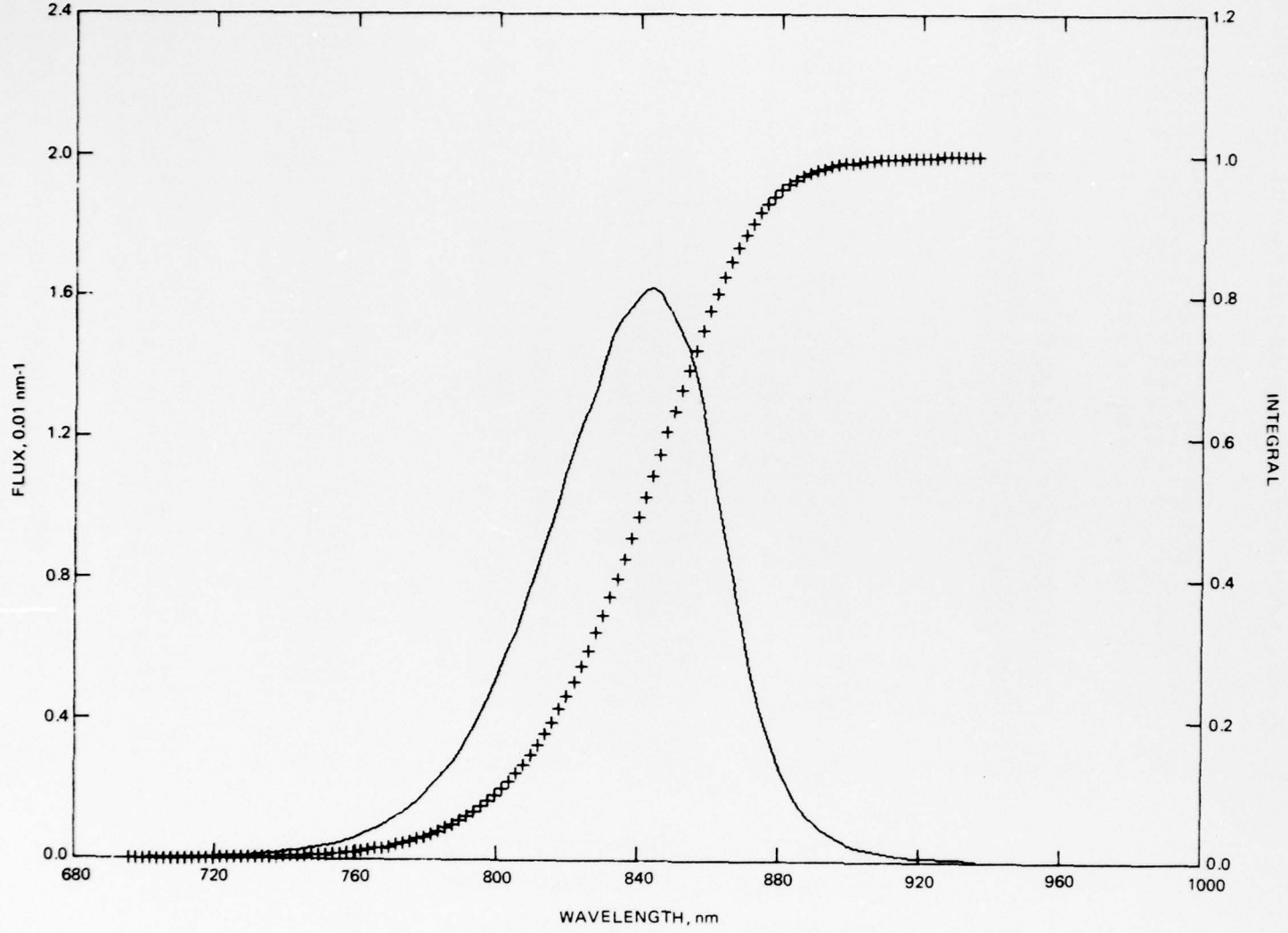

Figure 1(e). DSN122.S00.

Table 1(e). Relative spectral flux. Raw data file: DSN122.S00.

PEAK WAVELENGTH: 844.00 NM

AVERAGE WAVELENGTH: 840.86 NM

SPECTRAL WIDTH (FWHM): 55.71 NM

WAVELENGTH (NM)	FLUX (NM-1)	INTEGRAL	WAVELENGTH (NM)	FLUX (NM-1)	INTEGRAL	WAVELENGTH (NM)	FLUX (NM-1)	INTEGRAL
695.79	0.00001	0.00000	697.79	0.00001	0.00005	699.79	0.00000	0.00011
701.79	0.00002	0.00018	703.79	0.00002	0.00025	705.79	0.00003	0.00033
707.79	0.00003	0.00041	709.79	0.00003	0.00049	711.79	0.00004	0.00058
713.79	0.00004	0.00067	715.79	0.00004	0.00076	717.79	0.00005	0.00087
719.79	0.00006	0.00099	721.79	0.00006	0.00113	723.79	0.00008	0.00129
725.79	0.00008	0.00147	727.79	0.00009	0.00166	729.79	0.00010	0.00187
731.79	0.00012	0.00209	733.79	0.00014	0.00235	735.79	0.00015	0.00263
737.79	0.00017	0.00296	739.79	0.00019	0.00333	741.79	0.00022	0.00376
743.79	0.00026	0.00423	745.79	0.00028	0.00477	747.79	0.00031	0.00536
749.79	0.00034	0.00601	751.79	0.00039	0.00675	753.79	0.00044	0.00758
755.79	0.00049	0.00850	757.79	0.00055	0.00953	759.79	0.00061	0.01070
761.79	0.00070	0.01202	763.79	0.00078	0.01349	765.79	0.00087	0.01512
767.79	0.00098	0.01692	769.80	0.00111	0.01893	771.80	0.00124	0.02114
773.81	0.00138	0.02360	775.81	0.00151	0.02632	777.82	0.00169	0.02938
779.82	0.00188	0.03276	781.82	0.00210	0.03648	783.83	0.00232	0.04062
785.83	0.00255	0.04520	787.84	0.00281	0.05028	789.84	0.00313	0.05580
791.85	0.00346	0.06190	793.85	0.00380	0.06859	795.86	0.00419	0.07599
797.86	0.00462	0.08404	799.87	0.00514	0.09283	801.87	0.00562	0.10235
803.88	0.00611	0.11286	805.88	0.00658	0.12430	807.89	0.00715	0.13670
809.90	0.00782	0.15004	811.90	0.00842	0.16437	813.91	0.00903	0.18003
815.91	0.00963	0.19694	817.92	0.01033	0.21507	819.92	0.01108	0.23408
821.93	0.01178	0.25430	823.93	0.01237	0.27576	825.94	0.01287	0.29879
827.95	0.01342	0.32301	829.95	0.01411	0.34793	831.96	0.01478	0.37378
833.96	0.01523	0.40051	835.97	0.01546	0.42857	837.98	0.01573	0.45767
839.98	0.01598	0.48707	841.99	0.01622	0.51672	844.00	0.01626	0.54659
846.00	0.01607	0.57673	848.01	0.01573	0.60744	850.01	0.01540	0.63791
852.02	0.01498	0.66779	854.02	0.01451	0.69658	856.02	0.01385	0.72470
858.03	0.01290	0.75243	860.03	0.01171	0.77926	862.03	0.01047	0.80466
864.04	0.00942	0.82826	866.04	0.00842	0.84982	868.05	0.00741	0.86982
870.05	0.00631	0.88812	872.05	0.00529	0.90466	874.06	0.00446	0.91930
876.06	0.00378	0.93186	878.07	0.00321	0.94264	880.07	0.00268	0.95176
882.08	0.00222	0.95952	884.08	0.00183	0.96605	886.09	0.00153	0.97155
888.09	0.00129	0.97608	890.10	0.00110	0.97981	892.10	0.00093	0.98285
894.10	0.00080	0.98538	896.11	0.00068	0.98756	898.11	0.00058	0.98941
900.11	0.00048	0.99096	902.12	0.00041	0.99226	904.12	0.00036	0.99335
906.13	0.00032	0.99430	908.13	0.00028	0.99512	910.13	0.00024	0.99584
912.14	0.00020	0.99646	914.14	0.00018	0.99700	916.14	0.00016	0.99746
918.14	0.00014	0.99787	920.15	0.00013	0.99823	922.15	0.00011	0.99855
924.15	0.00010	0.99884	926.15	0.00009	0.99910	928.15	0.00008	0.99933
930.15	0.00007	0.99953	932.15	0.00006	0.99971	934.15	0.00006	0.99986
936.15	0.00005	1.00000						

FAR-FIELD MEASUREMENTS

The radiant flux emitted by an LED into the hemisphere in front of it varies from point to point on the hemisphere and often presents a pattern unique to the individual LED being measured. Two diodes that emit the same total flux could therefore contain markedly different amounts of flux within a cone of a given half-angle, θ, and would therefore couple different amounts of flux into an optical fiber with a given numerical aperture. The amount of flux actually contained within a cone of half-angle θ can be found from the far-field measurements presented in this section.

The far-field measurements consist of a record of the angular distribution of radiant intensity of each diode. These measurements are performed by holding the diode in a goniometer capable of obeying computer commands to move to a given position defined by polar angle θ and azimuthal angle ϕ. The geometry of the far-field goniometer is shown in appendix A. A calibrated detector is placed at a distance D far enough away from the LED so that the active area of the detector subtends a small solid angle (on the order of 10^{-3} sr) at the LED. With a dc current of 100 mA through the diode, and with the goniometer "on-axis" (θ and ϕ both zero), the absolute flux falling on the detector is measured by recording the dc signal $i(0^\circ, 0^\circ)$ from the detector. Following this, the LED current is changed to a square wave at 10^4 Hz (that is, the bias is chopped electrically) and the ac signal from the detector is rectified by a lock-in amplifier, digitized, and stored in computer memory as the first entry of the far-field pattern, $m(0^\circ, 0^\circ)$. The goniometer then moves the diode to a new polar angle (2 degrees in this case) and records the second entry $m(2^\circ, 0^\circ)$. The entire far-field pattern is automatically scanned in this manner by incrementing the polar angle from 0° to 90° in 2° steps and the azimuthal angle from 0° to 360° in $22\frac{1}{2}^\circ$ steps. The series of entries $m(\theta, \phi)$, when divided by the first entry $m(0^\circ, 0^\circ)$, then represents the relative radiant intensity of the diode at each position on the hemisphere.

Figures 2(a), (b), (c), and (e) show a section plot of the relative radiant intensity of diodes a, b, c and e. In these plots, the line of the emitter axis $(\theta, \phi) = (0^\circ, 0^\circ)$ points vertically upward, θ is measured in a positive sense from the emitter axis to the direction of observation, and ϕ is measured positive in a counterclockwise sense looking along the axis into the emitter. Figures 3(a), (b), (c), and (e) represent the same data in the form of a grey scale plot. In this plot, light areas are high intensity, dark areas are low intensity, constant azimuth lines are radial, and constant polar angle lines are circular. The coordinates for the grey scale plot are given in appendix B. These figures provide a contour plot superimposed on the grey scale representation. Each contour represents the locus of a level of constant radiant intensity.

The relative far-field pattern can be converted to an absolute one by using the on-axis dc measurement. A major assumption of this conversion is separability, namely that the spectral radiant intensity $I_\lambda(\theta, \phi, \lambda)$ W sr^{-1} nm^{-1} can be written as the product of a purely angular function $\Theta(\theta, \phi)$ in sr^{-1}, a purely spectral function $\Lambda(\lambda)$ in nm^{-1} and a single constant Φ in W: $I_\lambda(\theta, \phi, \lambda) \equiv \partial^2 P/\partial\Omega\partial\lambda = \Phi \cdot \Theta(\theta, \phi) \cdot \Lambda(\lambda)$.* This means that the spectrum is independent of the angle at which it is observed. A minor assumption is that ac operation of the diode does not alter the relative radiant intensity. That is, it is assumed that $m(\theta, \phi)/m(0^\circ, 0^\circ) \equiv \Theta(\theta, \phi)/\Theta(0^\circ, 0^\circ)$. With these assumptions it can then be shown that the radiant intensity $I(\theta, \phi) \equiv \partial P/\partial\Omega$ in W sr^{-1} is given by

*P is the radiant flux in watts emitted by the diode.

$$I(\theta, \phi) = \left\{ \frac{D^2 \quad i(0^\circ, 0^\circ)}{\int R(\lambda)\Lambda(\lambda)d\lambda} \right\} \left\{ \frac{m(\theta \quad \phi)}{m(0^\circ, 0^\circ)} \right\}$$

In this equation, $\Lambda(\lambda)$ is the normalized spectral flux presented in the previous section and $R(\lambda)$ is the absolute response of the detector in A cm^2 W^{-1}. The first bracket is the total on-axis dc radiant intensity $\Phi \cdot \Theta(0^\circ, 0^\circ)$, and the second bracket is the relative ac far-field pattern. The integral over solid angle can be performed in two steps, first over azimuthal angle ϕ and then over polar angle θ. The integral over ϕ determines a function $G(\theta)$ which we have called the polar radiant intensity:

$$G(\theta) \equiv \int_0^{2\pi} I(\theta, \phi)d\phi = \Phi \cdot \Theta(0^\circ, 0^\circ) \int_0^{2\pi} \frac{m(\theta, \phi)}{m(0^\circ, 0^\circ)} d\phi$$

The meaning of this function is that $G(\theta) \sin \theta \, d\theta$ is the amount of flux contained between polar angles θ and $\theta + d\theta$. The solid lines in figures 4(a), (b), (c), and (e) are plots of $G(\theta)$ in mW deg^{-1}.

The integral of $G(\theta) \sin(\theta)$ over θ determines the total flux contained within a cone of half-angle θ. We have called this integral the conical radiant flux. It is shown in milliwatts in figures 4(a), (b), (c), and (e) by the string of crosses.

Tables 2(a), (b), (c), and (e) represent the data of figures 4(a), (b), (c), and (e) in tabular form. The hemispherical flux is the total flux emitted by the diode into the forward hemisphere. The half-flux angle is the half-angle of a cone dividing the total flux into two equal parts; half the flux lies inside this cone, and half lies outside this cone.

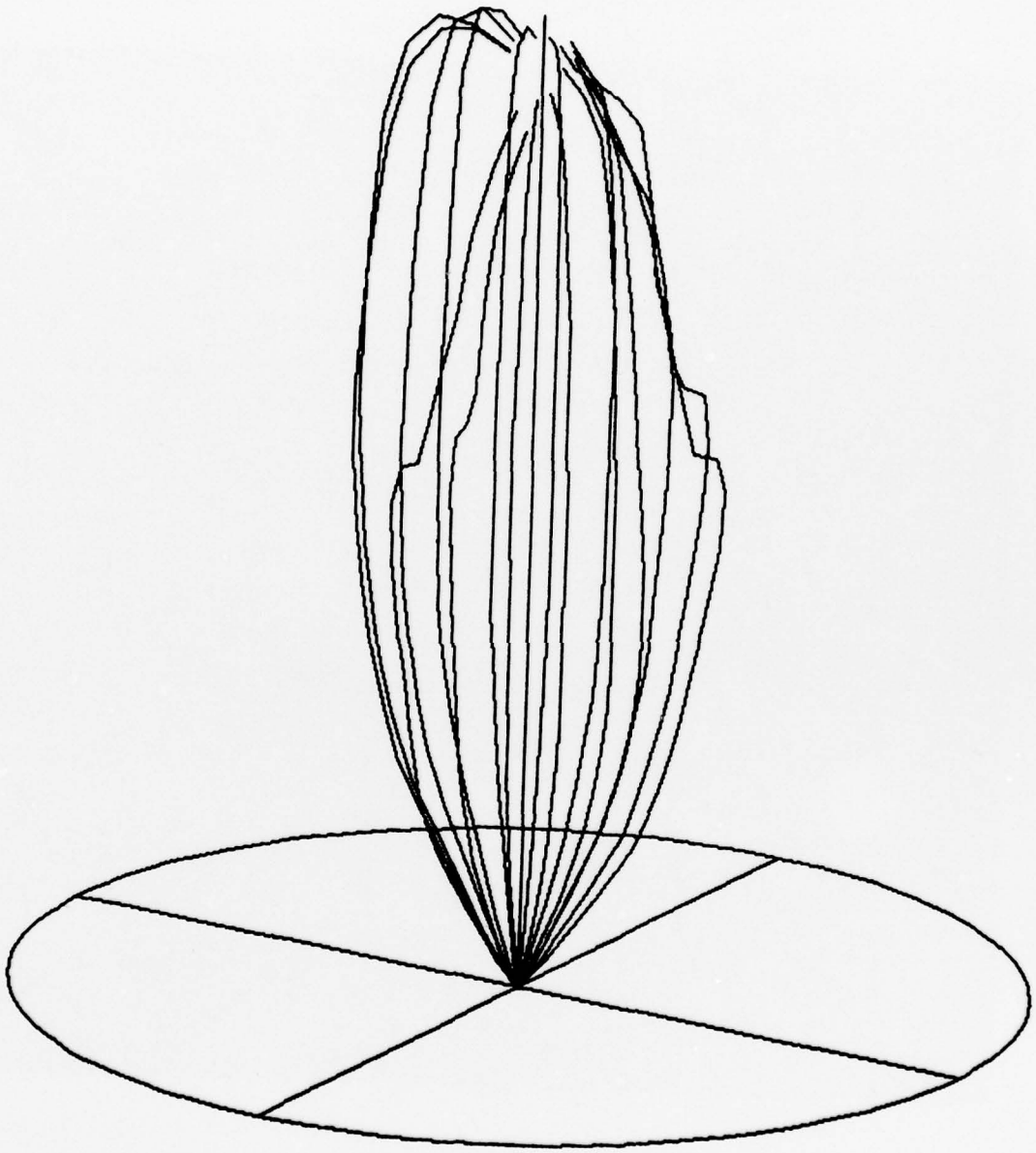

Figure 2(a). DSN118.FF4.

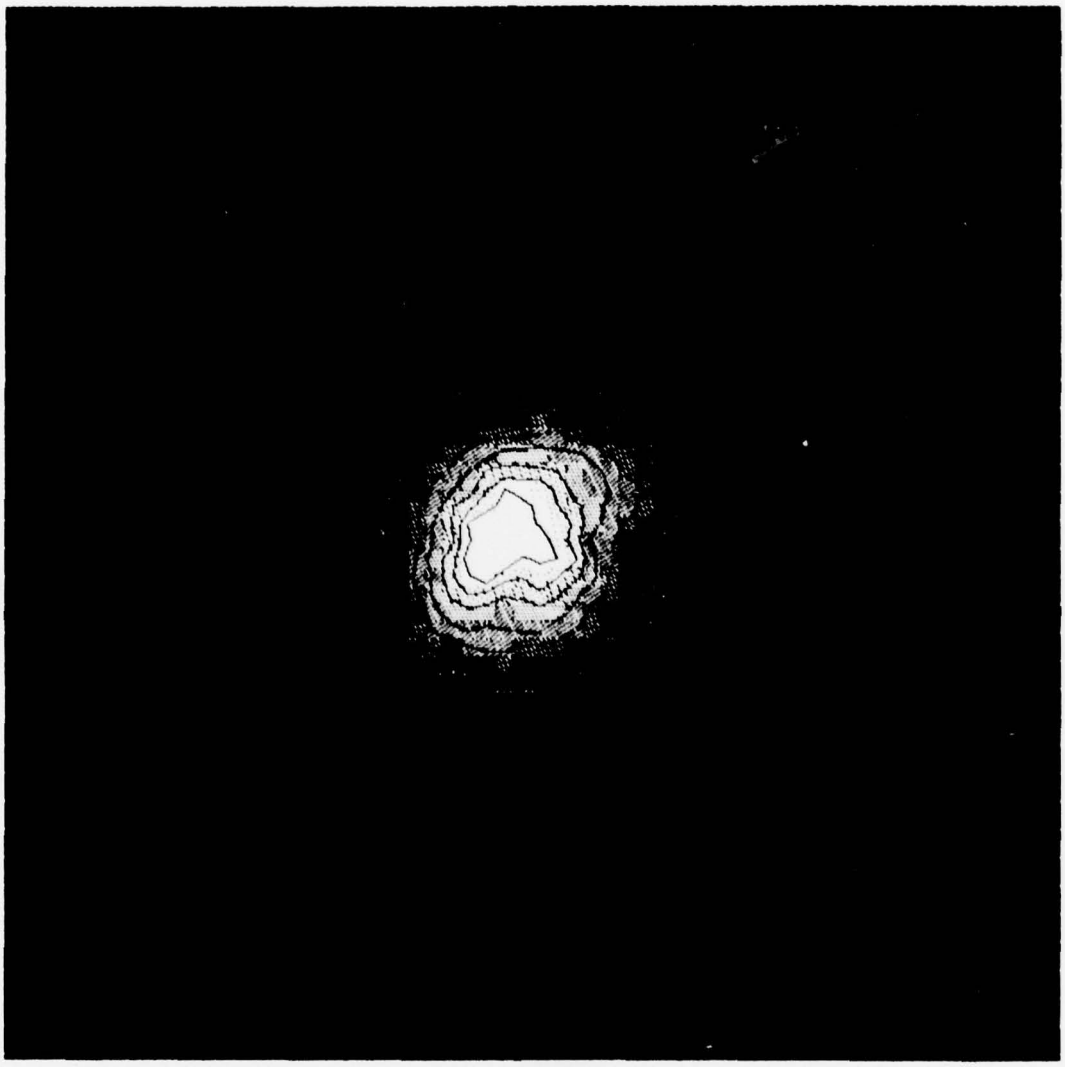

Figure 3(a). DSN 18 EE4.

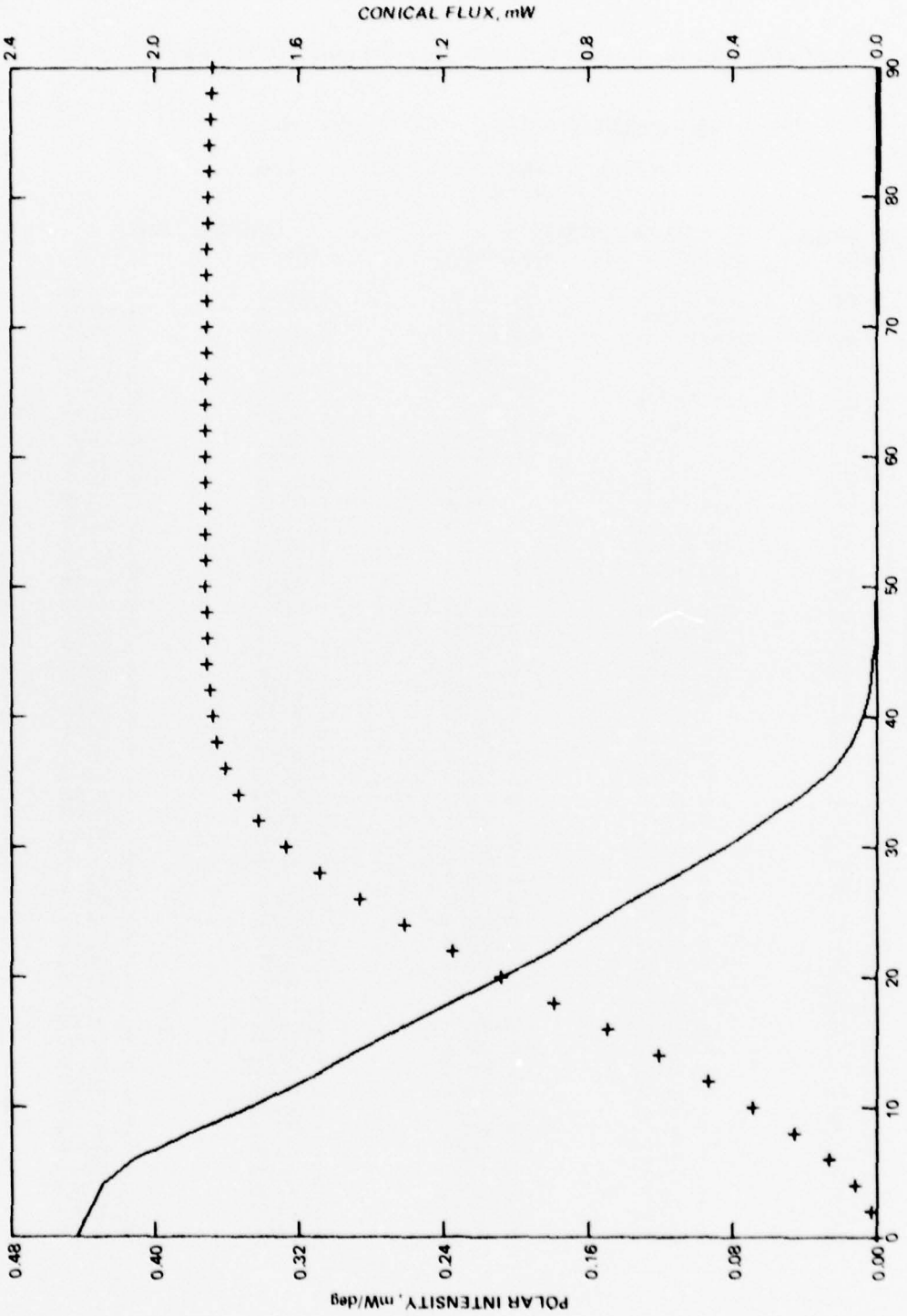

Figure 4(a). DSN118.FF4.

Table 2(a). Angular radiant intensity. Raw data file: DSN118.FF4.

HEMISPHERICAL FLUX: 1.839 MW

HALF-FLUX ANGLE: 18.3 DEG

POLAR ANGLE (DEG)	POLAR INTENSITY (UW/DEG)	(MW/RADIAN)	CONICAL FLUX (MW)	(--)
0.00	442.9119	25.3770	0.0000	0.0000
2.00	436.5589	25.0130	0.0152	0.0083
4.00	429.5601	24.6120	0.0604	0.0329
6.00	411.1818	23.5590	0.1334	0.0725
8.00	380.2372	21.7860	0.2293	0.1247
10.00	347.0934	19.8870	0.3425	0.1863
12.00	317.0214	18.1640	0.4687	0.2549
14.00	291.7490	16.7160	0.6051	0.3291
16.00	264.9757	15.1820	0.7488	0.4073
18.00	236.1778	13.5320	0.8948	0.4867
20.00	207.1879	11.8710	1.0386	0.5649
22.00	180.9905	10.3700	1.1773	0.6403
24.00	158.0796	9.0573	1.3094	0.7122
26.00	135.2681	7.7503	1.4330	0.7794
28.00	108.5175	6.2176	1.5432	0.8393
30.00	84.0480	4.8156	1.6362	0.8899
32.00	62.6974	3.5923	1.7115	0.9309
34.00	41.7744	2.3936	1.7680	0.9616
36.00	24.0349	1.3771	1.8055	0.9820
38.00	13.9120	0.7971	1.8282	0.9943
40.00	7.9973	0.4582	1.8419	1.0018
42.00	4.2579	0.2440	1.8499	1.0061
44.00	2.0672	0.1184	1.8542	1.0085
46.00	0.9750	0.0559	1.8563	1.0096
48.00	0.5238	0.0300	1.8574	1.0102
50.00	0.3507	0.0201	1.8581	1.0106
52.00	0.2404	0.0138	1.8585	1.0108
54.00	0.1557	0.0089	1.8589	1.0110
56.00	0.0896	0.0051	1.8591	1.0111
58.00	0.0395	0.0023	1.8592	1.0112
60.00	-0.0259	-0.0015	1.8592	1.0112
62.00	-0.0947	-0.0054	1.8591	1.0111
64.00	-0.1716	-0.0098	1.8588	1.0110
66.00	-0.2414	-0.0138	1.8585	1.0108
68.00	-0.3119	-0.0179	1.8579	1.0105
70.00	-0.3901	-0.0224	1.8573	1.0102
72.00	-0.4504	-0.0258	1.8565	1.0097
74.00	-0.5419	-0.0310	1.8555	1.0092
76.00	-0.6682	-0.0383	1.8544	1.0086
78.00	-0.8445	-0.0484	1.8529	1.0078
80.00	-1.0104	-0.0579	1.8511	1.0068
82.00	-1.2162	-0.0697	1.8489	1.0056
84.00	-1.2867	-0.0737	1.8464	1.0042
86.00	-1.2970	-0.0743	1.8438	1.0028
88.00	-1.3104	-0.0751	1.8412	1.0014
90.00	-1.3208	-0.0757	1.8386	1.0000

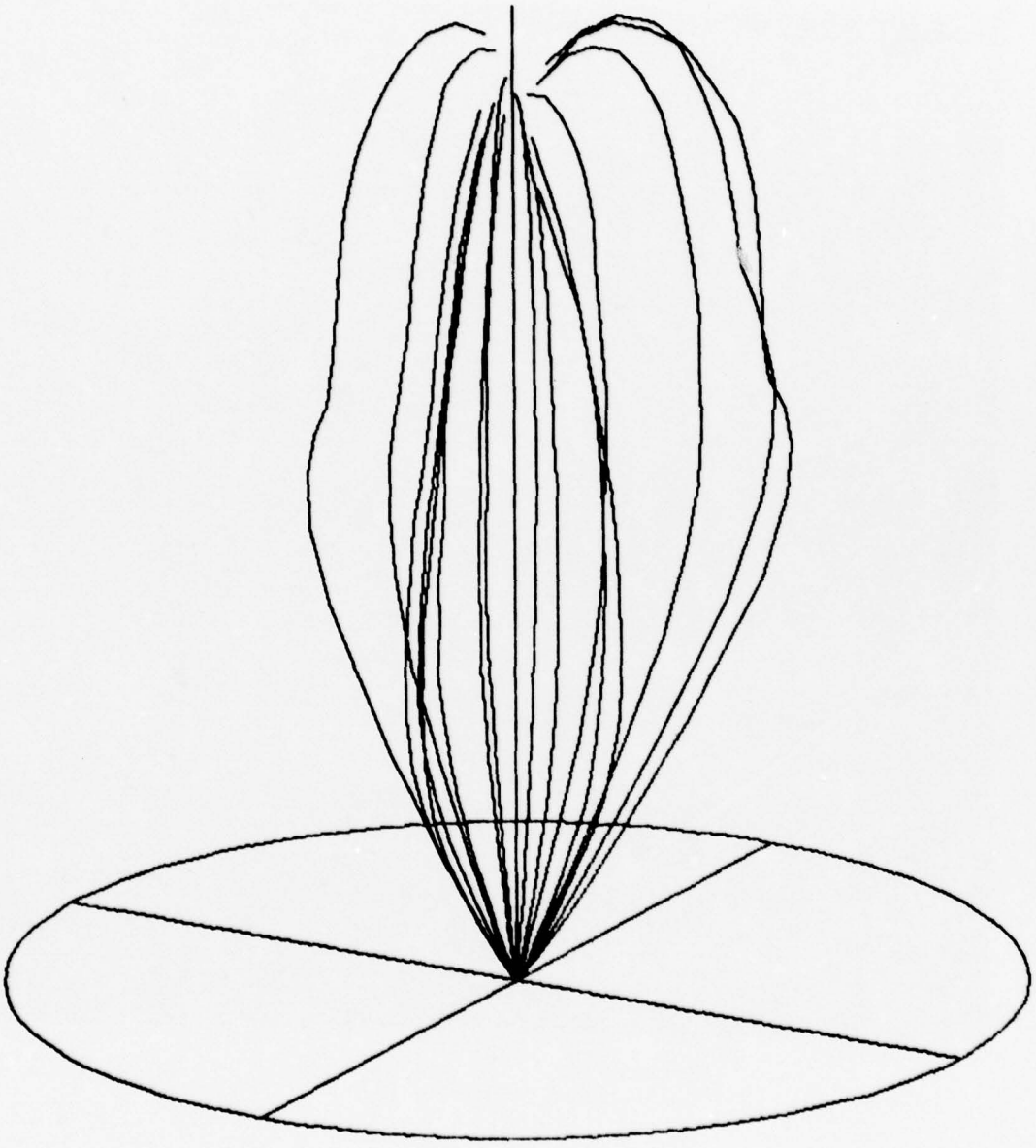

Figure 2(b). DSN119.FF3.

Figure 3(b) $^{15}N119FF3$.

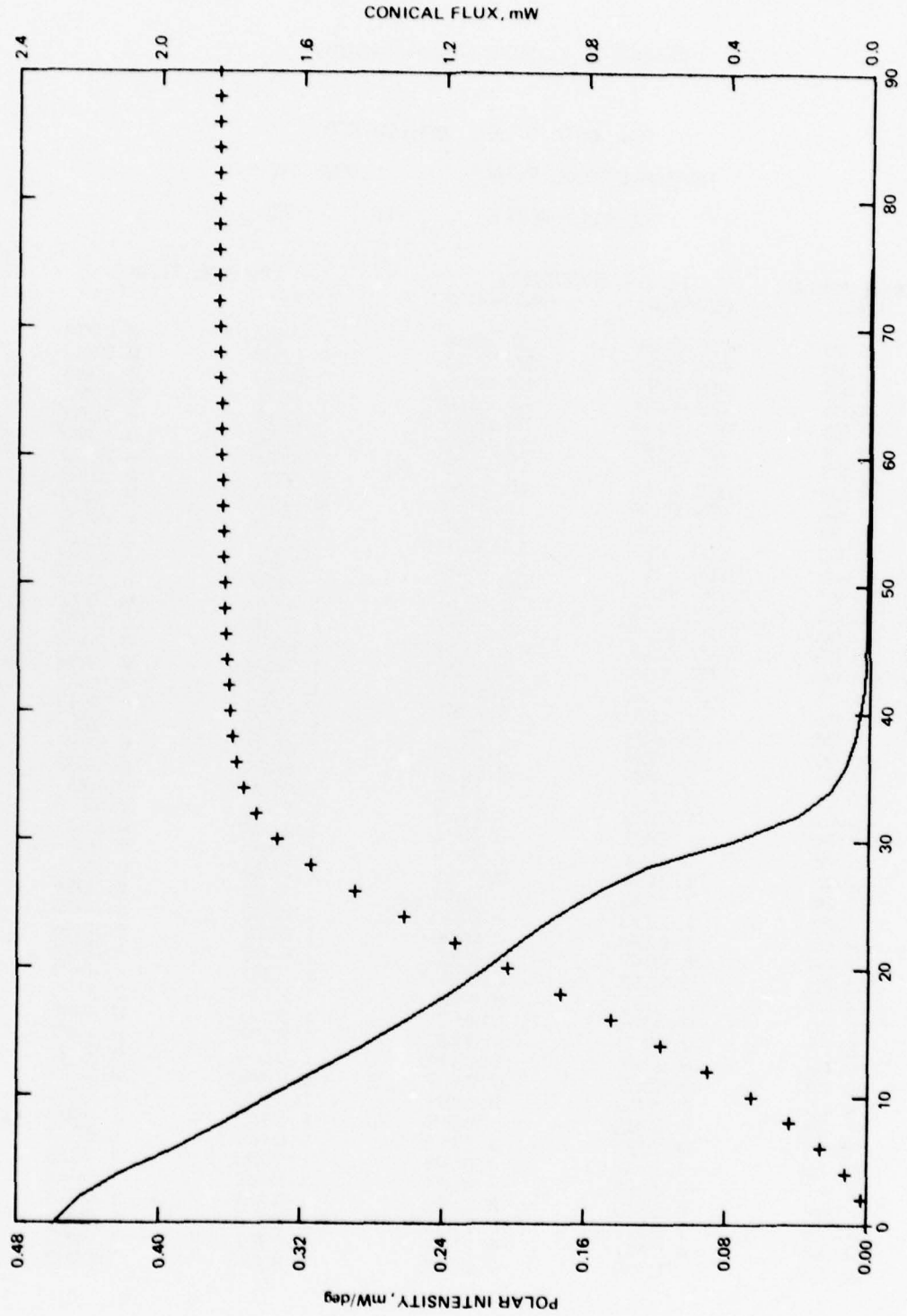

Figure 4(b). DSN119.FF3.

Table 2(b). Angular radiant intensity.

RAW DATA FILE: DSN119.FF3

HEMISPHERICAL FLUX: 1.839 MW

HALF-FLUX ANGLE: 18.7 DEG

POLAR ANGLE (DEG)	POLAR INTENSITY (UW/DEG)	(MW/RADIAN)	CONICAL FLUX (MW)	(--)
0.00	458.7420	26.2840	0.0000	0.0000
2.00	444.2558	25.4540	0.0155	0.0084
4.00	420.2051	24.0760	0.0603	0.0328
6.00	388.1784	22.2410	0.1302	0.0708
8.00	361.2654	20.6990	0.2211	0.1202
10.00	335.6440	19.2310	0.3296	0.1793
12.00	309.3070	17.7220	0.4522	0.2460
14.00	283.3714	16.2360	0.5851	0.3182
16.00	259.0939	14.8450	0.7250	0.3943
18.00	236.4745	13.5490	0.8695	0.4729
20.00	215.2862	12.3350	1.0162	0.5527
22.00	196.4367	11.2550	1.1635	0.6328
24.00	176.4527	10.1100	1.3088	0.7118
26.00	152.8995	8.7605	1.4476	0.7873
28.00	124.2272	7.1177	1.5730	0.8555
30.00	77.0108	4.4124	1.6698	0.9082
32.00	39.8389	2.2826	1.7294	0.9406
34.00	21.5792	1.2364	1.7626	0.9587
36.00	12.8290	0.7351	1.7822	0.9693
38.00	8.1699	0.4681	1.7948	0.9762
40.00	5.2938	0.3033	1.8032	0.9807
42.00	3.5085	0.2010	1.8089	0.9838
44.00	2.5143	0.1441	1.8130	0.9861
46.00	1.8398	0.1054	1.8161	0.9878
48.00	1.5723	0.0901	1.8186	0.9891
50.00	1.4301	0.0819	1.8209	0.9904
52.00	1.3138	0.0753	1.8230	0.9915
54.00	1.2106	0.0694	1.8250	0.9926
56.00	1.1223	0.0643	1.8269	0.9936
58.00	1.0392	0.0595	1.8287	0.9946
60.00	0.9647	0.0553	1.8305	0.9956
62.00	0.8818	0.0505	1.8321	0.9965
64.00	0.7992	0.0458	1.8336	0.9973
66.00	0.7384	0.0423	1.8350	0.9980
68.00	0.6733	0.0386	1.8363	0.9987
70.00	0.6001	0.0344	1.8374	0.9993
72.00	0.5365	0.0307	1.8385	0.9999
74.00	0.4659	0.0267	1.8395	1.0005
76.00	0.3755	0.0215	1.8403	1.0009
78.00	0.1253	0.0072	1.8408	1.0012
80.00	-0.1036	-0.0059	1.8408	1.0012
82.00	-0.2164	-0.0124	1.8405	1.0010
84.00	-0.2306	-0.0132	1.8400	1.0008
86.00	-0.2327	-0.0133	1.8396	1.0005
88.00	-0.2401	-0.0138	1.8391	1.0003
90.00	-0.2350	-0.0135	1.8386	1.0000

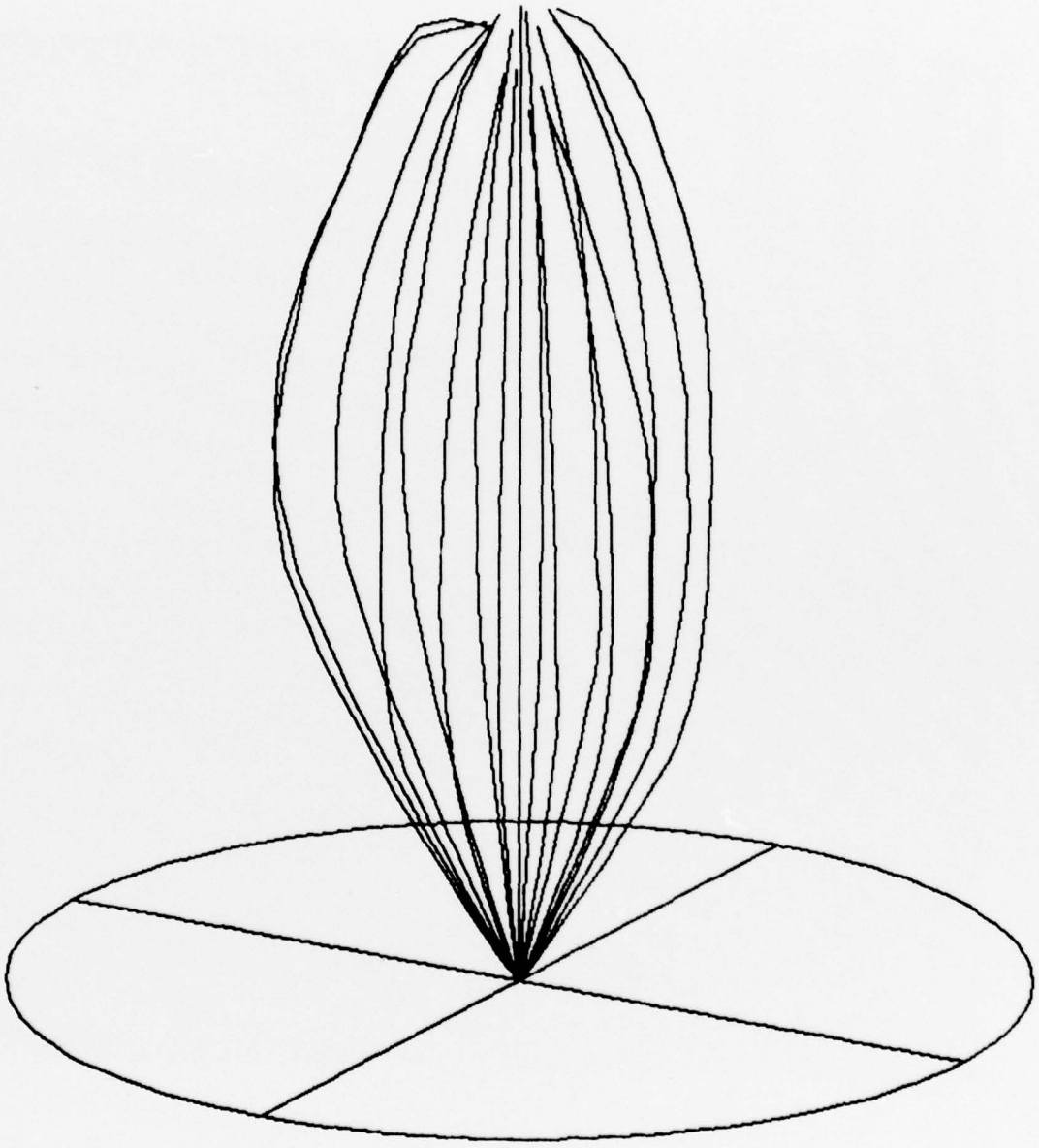

Figure 2(c). DSN120.FF3.

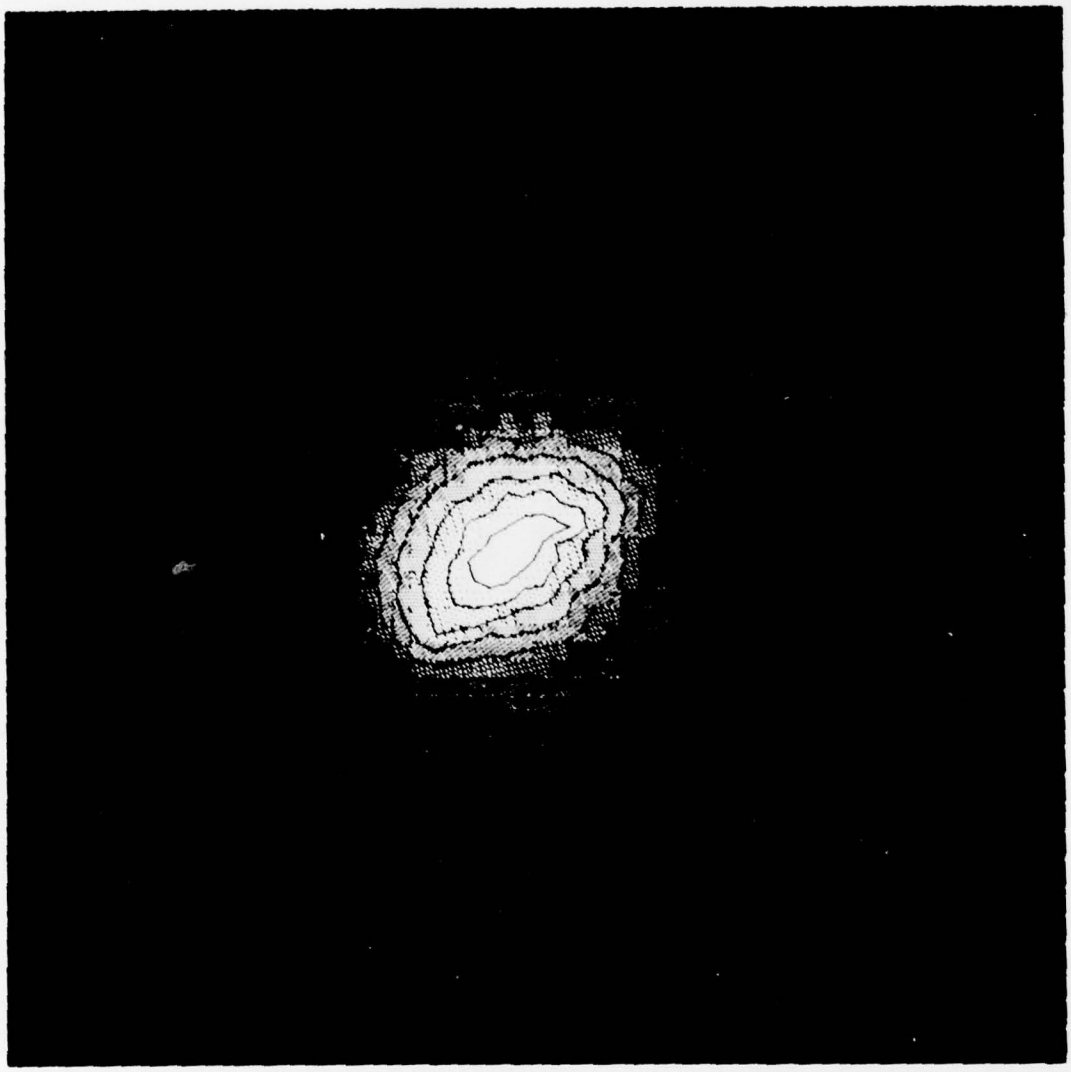

Figure 3(c). DSN120.FF3.

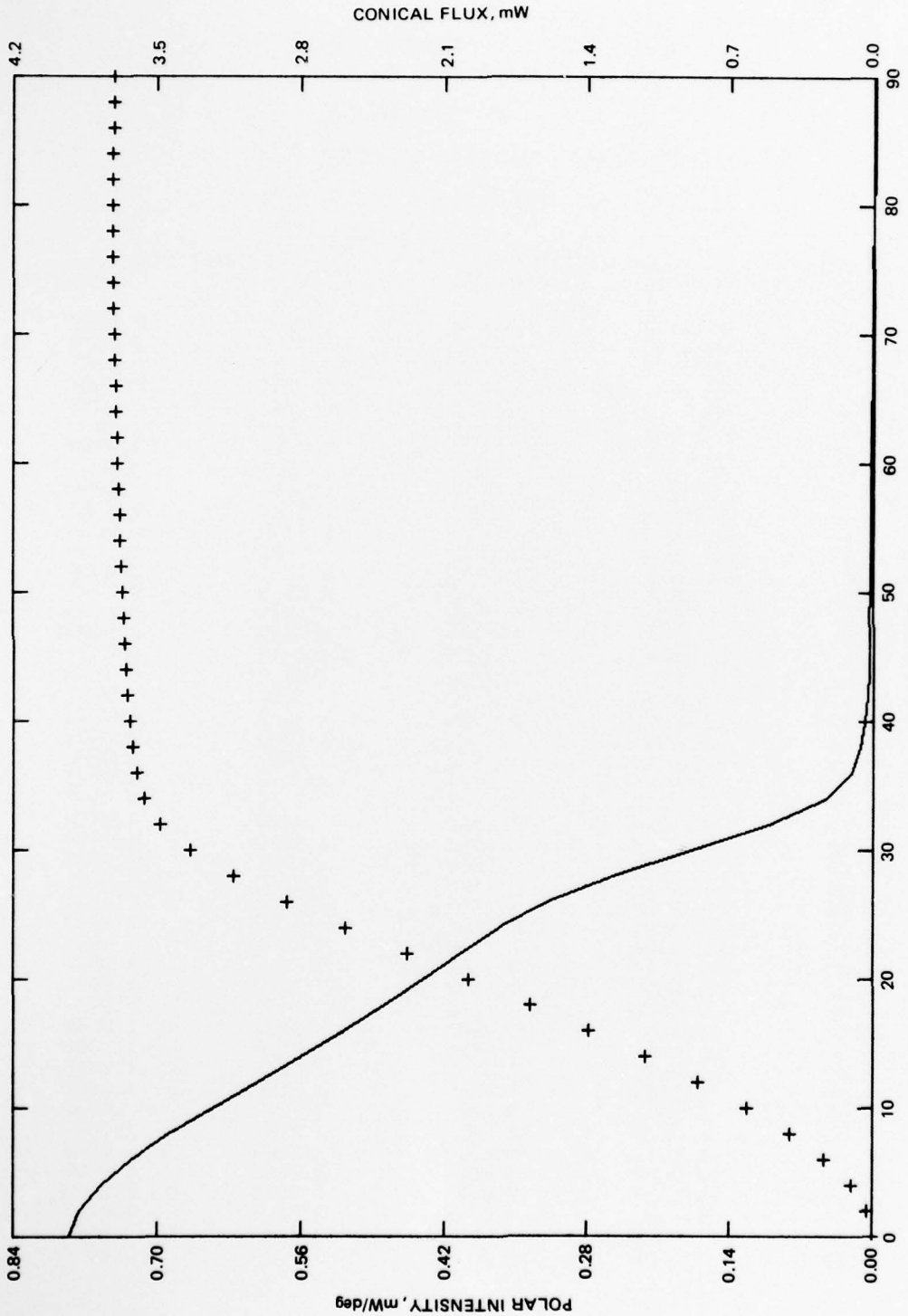

Figure 4(c). DSN120.FF3.

Table 2(c). Angular radiant intensity.

RAW DATA FILE: DSN120.FF3

HEMISPHERICAL FLUX: 3.708 MW

HALF-FLUX ANGLE: 19.2 DEG

POLAR ANGLE (DEG)	POLAR INTENSITY (UW/DEG)	(MW/RADIAN)	CONICAL FLUX (MW)	(--)
0.00	785.3452	44.9970	0.0000	0.0000
2.00	775.4143	44.4280	0.0271	0.0073
4.00	754.4354	43.2260	0.1067	0.0288
6.00	724.6602	41.5200	0.2351	0.0634
8.00	689.0729	39.4810	0.4068	0.1097
10.00	645.4921	36.9840	0.6148	0.1658
12.00	601.6495	34.4720	0.8519	0.2297
14.00	559.7615	32.0720	1.1125	0.3000
16.00	517.3326	29.6410	1.3905	0.3750
18.00	479.0052	27.4450	1.6811	0.4533
20.00	441.0793	25.2720	1.9800	0.5339
22.00	404.8114	23.1940	2.2825	0.6155
24.00	366.3618	20.9910	2.5831	0.6966
26.00	319.0808	18.2820	2.8720	0.7745
28.00	255.0971	14.6160	3.1317	0.8445
30.00	177.7093	10.1820	3.3403	0.9007
32.00	101.6776	5.8257	3.4830	0.9392
34.00	46.2477	2.6498	3.5628	0.9607
36.00	21.2668	1.2185	3.6011	0.9711
38.00	12.4363	0.7125	3.6213	0.9765
40.00	8.4038	0.4815	3.6343	0.9800
42.00	6.0870	0.3488	3.6438	0.9826
44.00	4.8443	0.2776	3.6513	0.9846
46.00	4.1938	0.2403	3.6576	0.9863
48.00	3.7884	0.2171	3.6635	0.9879
50.00	3.4880	0.1998	3.6690	0.9894
52.00	3.2552	0.1865	3.6742	0.9908
54.00	3.0367	0.1740	3.6792	0.9921
56.00	2.8421	0.1628	3.6840	0.9934
58.00	2.6815	0.1536	3.6887	0.9947
60.00	2.5230	0.1446	3.6931	0.9959
62.00	2.3312	0.1336	3.6974	0.9970
64.00	2.1256	0.1218	3.7013	0.9981
66.00	1.9181	0.1099	3.7050	0.9991
68.00	1.6800	0.0963	3.7083	1.0000
70.00	1.4454	0.0828	3.7112	1.0008
72.00	1.2555	0.0719	3.7138	1.0015
74.00	1.0489	0.0601	3.7160	1.0020
76.00	0.7257	0.0416	3.7177	1.0025
78.00	0.0578	0.0033	3.7184	1.0027
80.00	-0.5612	-0.0322	3.7180	1.0026
82.00	-0.9500	-0.0544	3.7165	1.0022
84.00	-1.0134	-0.0581	3.7145	1.0016
86.00	-1.0168	-0.0583	3.7125	1.0011
88.00	-1.0339	-0.0592	3.7104	1.0005
90.00	-1.0366	-0.0594	3.7084	1.0000

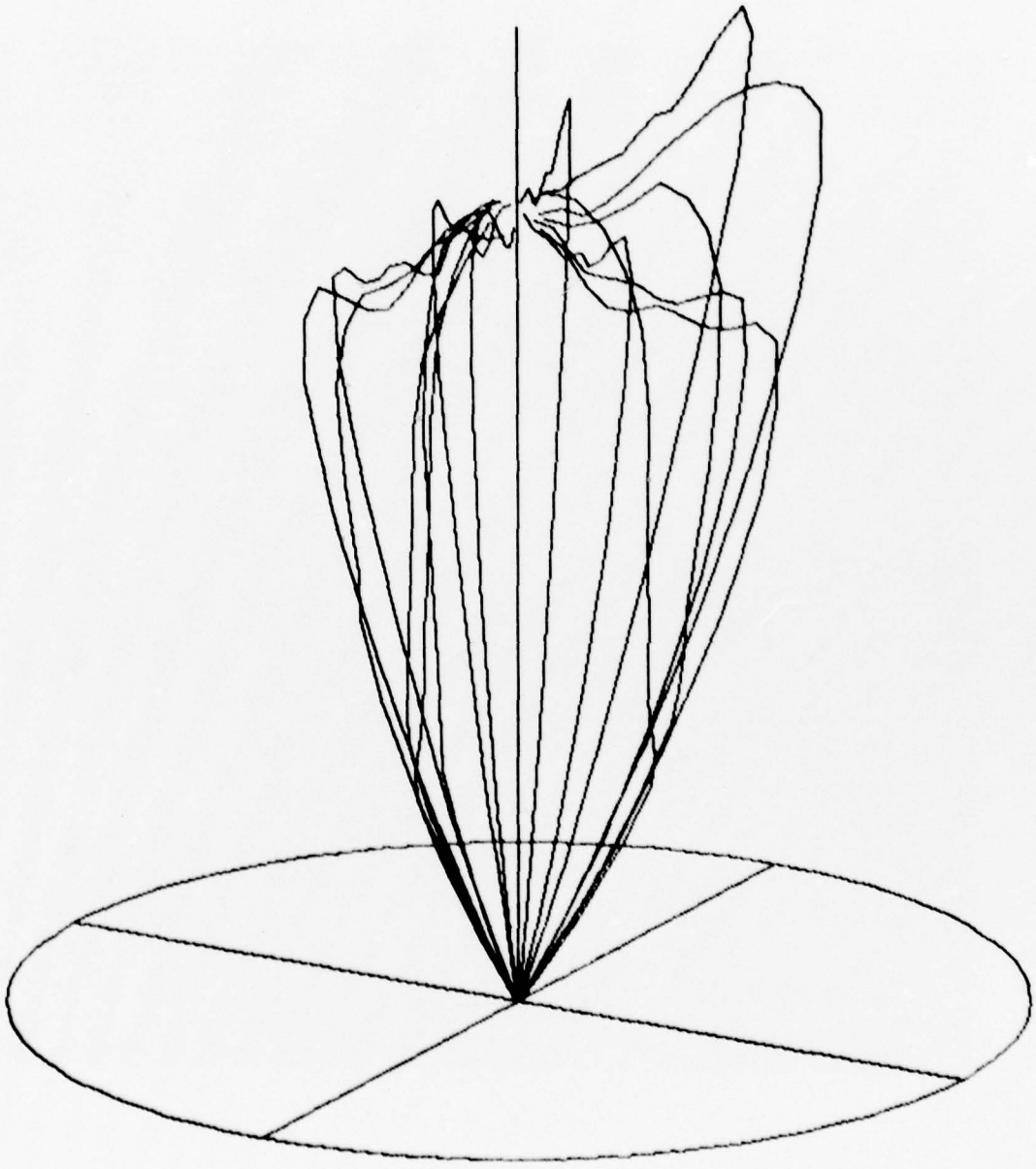

Figure 2(e). DSN122.FF2.

Figure 5(e). DSN 22 FF2.

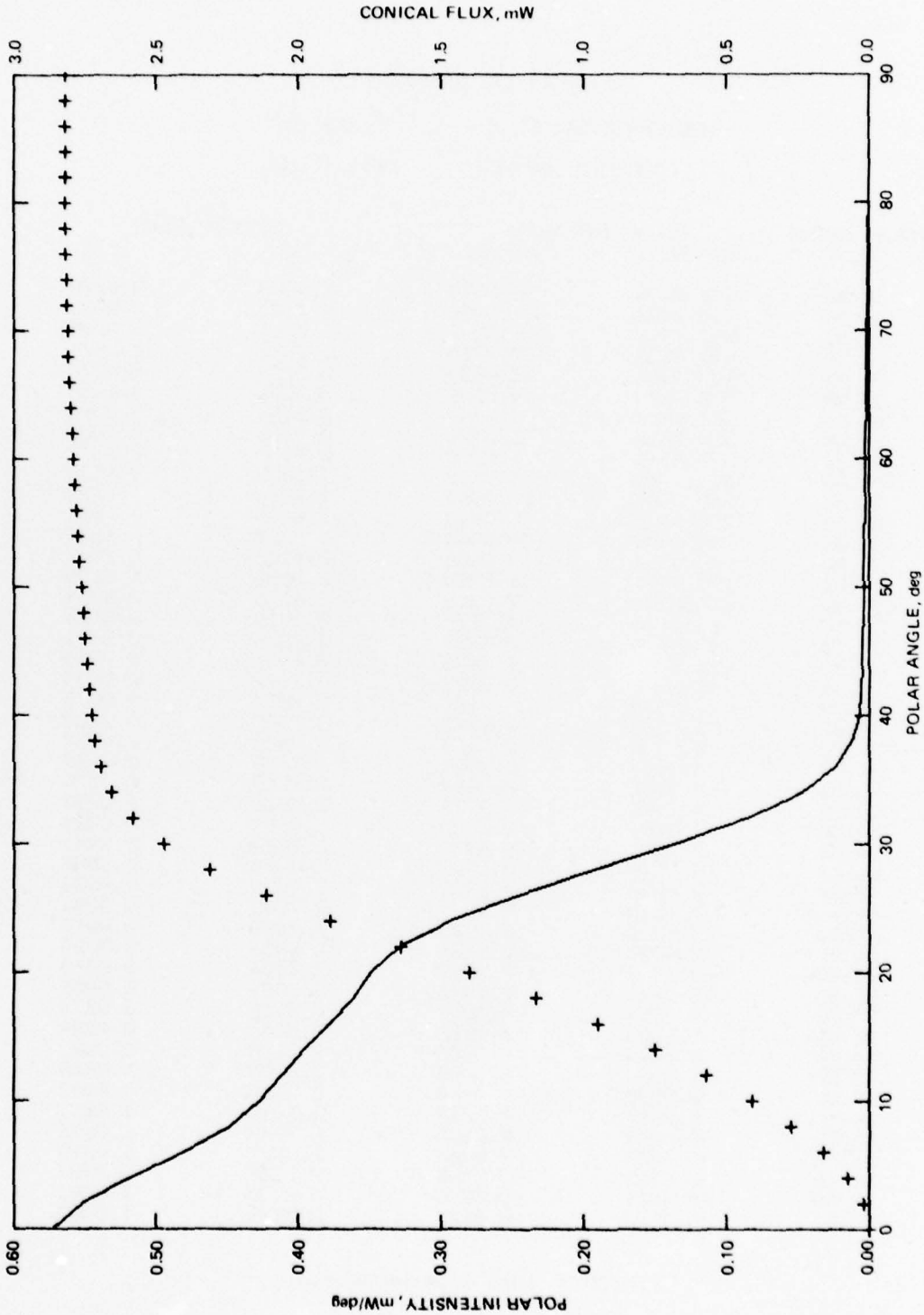

Figure 4(e). DSN122.FF2.

RAW DATA FILE: DSN122.FF2

HEMISPHERICAL FLUX: 2.819 MW

HALF-FLUX ANGLE: 20.1 DEG

POLAR ANGLE (DEG)	POLAR INTENSITY (UW/DEG)	(MW/RADIAN)	CONICAL FLUX (MW)	(--)
0.00	573.0261	32.8320	0.0000	0.0000
2.00	552.3788	31.6490	0.0193	0.0068
4.00	517.7341	29.6640	0.0747	0.0265
6.00	479.5638	27.4770	0.1609	0.0571
8.00	447.9908	25.6680	0.2734	0.0970
10.00	426.7850	24.4530	0.4099	0.1454
12.00	410.9200	23.5440	0.5694	0.2020
14.00	395.7880	22.6770	0.7506	0.2663
16.00	378.2126	21.6700	0.9506	0.3372
18.00	361.4749	20.7110	1.1665	0.4138
20.00	348.9609	19.9940	1.3976	0.4958
22.00	328.8372	18.8410	1.6401	0.5818
24.00	294.0878	16.8500	1.8829	0.6680
26.00	245.5327	14.0680	2.1102	0.7486
28.00	193.2951	11.0750	2.3086	0.8190
30.00	136.6854	7.8315	2.4676	0.8754
32.00	85.8178	4.9170	2.5815	0.9158
34.00	46.6474	2.6727	2.6530	0.9411
36.00	23.8691	1.3676	2.6931	0.9554
38.00	11.8792	0.6806	2.7145	0.9630
40.00	7.1639	0.4105	2.7264	0.9672
42.00	5.6259	0.3223	2.7348	0.9702
44.00	5.0532	0.2895	2.7420	0.9727
46.00	4.6454	0.2662	2.7489	0.9752
48.00	4.3591	0.2498	2.7555	0.9775
50.00	4.1176	0.2359	2.7619	0.9798
52.00	3.8966	0.2233	2.7681	0.9820
54.00	3.7003	0.2120	2.7742	0.9841
56.00	3.4640	0.1985	2.7800	0.9862
58.00	3.2030	0.1835	2.7856	0.9882
60.00	2.9370	0.1683	2.7909	0.9901
62.00	2.6805	0.1536	2.7958	0.9918
64.20	2.4099	0.1381	2.8003	0.9934
66.00	2.1344	0.1223	2.8044	0.9949
68.00	1.9042	0.1091	2.8081	0.9962
70.00	1.6695	0.0957	2.8115	0.9974
72.00	1.4166	0.0812	2.8144	0.9984
74.00	1.1948	0.0685	2.8169	0.9993
76.00	1.0160	0.0582	2.8190	1.0000
78.00	0.7780	0.0446	2.8208	1.0007
80.00	0.3807	0.0218	2.8219	1.0011
82.00	-0.1043	-0.0060	2.8222	1.0012
84.00	-0.4262	-0.0244	2.8217	1.0010
86.00	-0.4693	-0.0269	2.8208	1.0007
88.00	-0.4811	-0.0276	2.8198	1.0003
90.00	-0.4799	-0.0275	2.8189	1.0000

Table 2(e). Angular radiant intensity.

NEAR-FIELD MEASUREMENTS

This series of measurements consists of a microscope scan across the glass window of the diode. The diode is mounted vertically on a pair of tables capable of translating the diode in 0.1-mil steps in the X and Y directions under computer control. The diode is excited with a 10^4 Hz square wave. The optical radiation leaving the diode is collected with a 10X 0.2 N. A. microscope objective and focused onto an 8-mil aperture in front of a silicon photodiode, defining a field of 0.8 mil in diameter at the LED window itself. The signal due to the flux from this field is sensed by a lock-in amplifier, digitized, and stored in computer memory. The tables are then stepped through a sequence of positions causing the diode to move through the stationary field. The entire operation is equivalent to the scan of an 0.8-mil photosensitive spot in the X and Y directions across the face of the diode window.

Near-field scans were performed with 1.0-mil steps in X and Y covering a 25-mil square.

The data from the near-field scans are presented from three different points of view. Figures 5(a) – (e) are perspective section plots in which intensity increases in the vertical direction. Figures 6(a) – (e) are contour plots showing lines of equal intensity superimposed upon a grey scale plot of the near-field data. Figures 7(a) – (e) are graphs whose ordinate is the amount of flux contained within a circle centered on the intensity centroid and whose abscissa is the diameter of the circle.

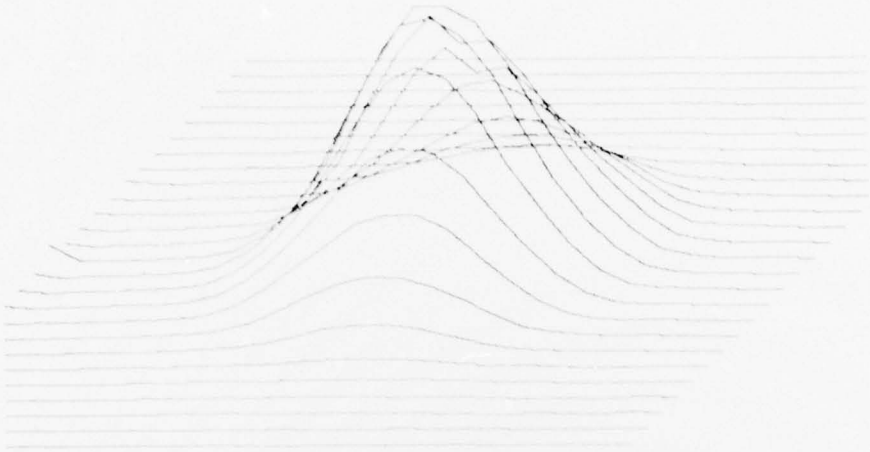

Figure 5(a). DSN118.NET.

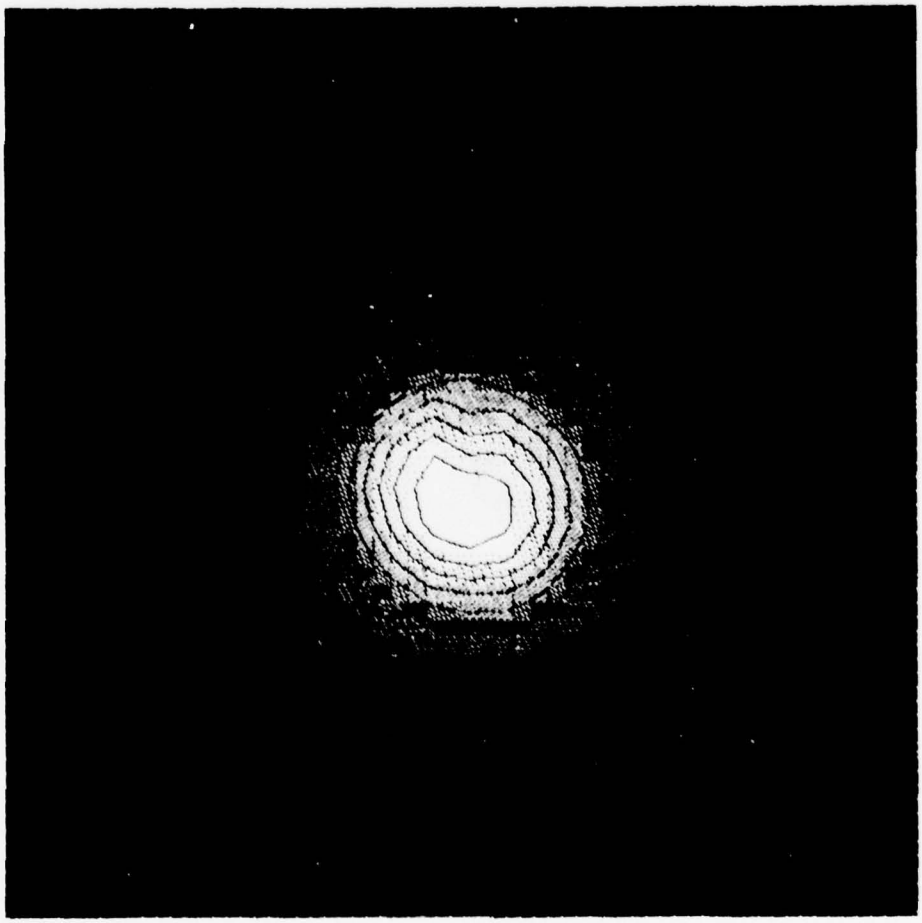

Figure 6(a). DSN118.NET.

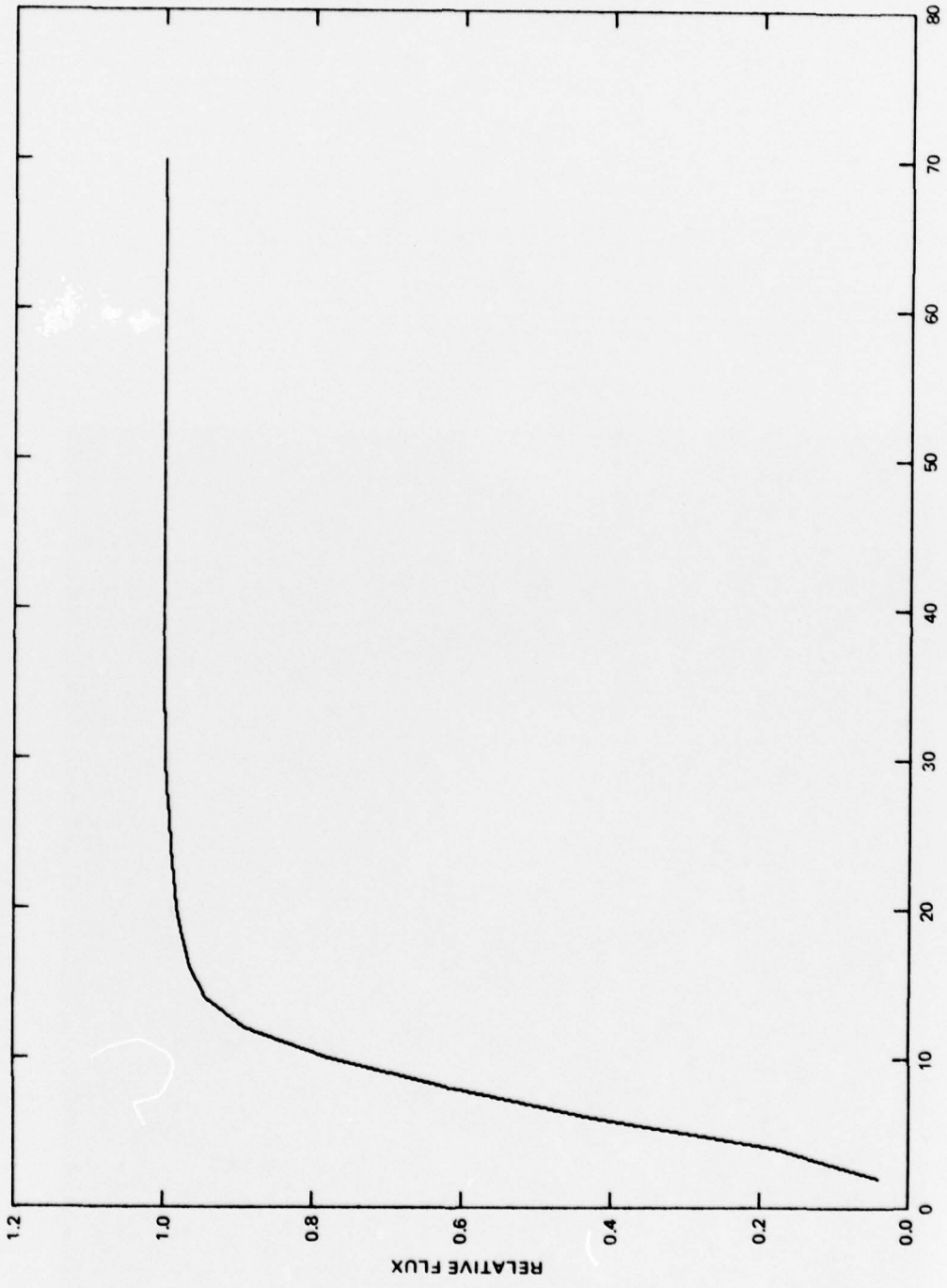

Figure 7(a). DSN118.NF1.

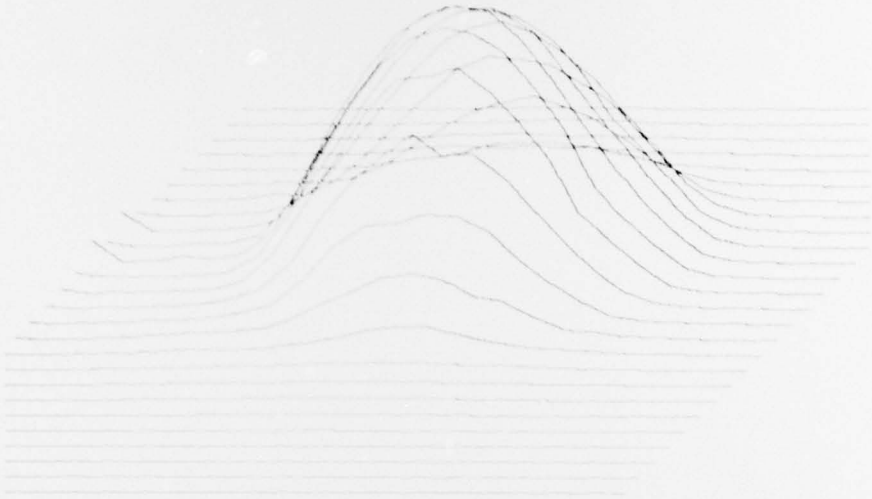

Figure 5(b). DSN119.NF0.

Figure 6(b). DSN119.NF0.

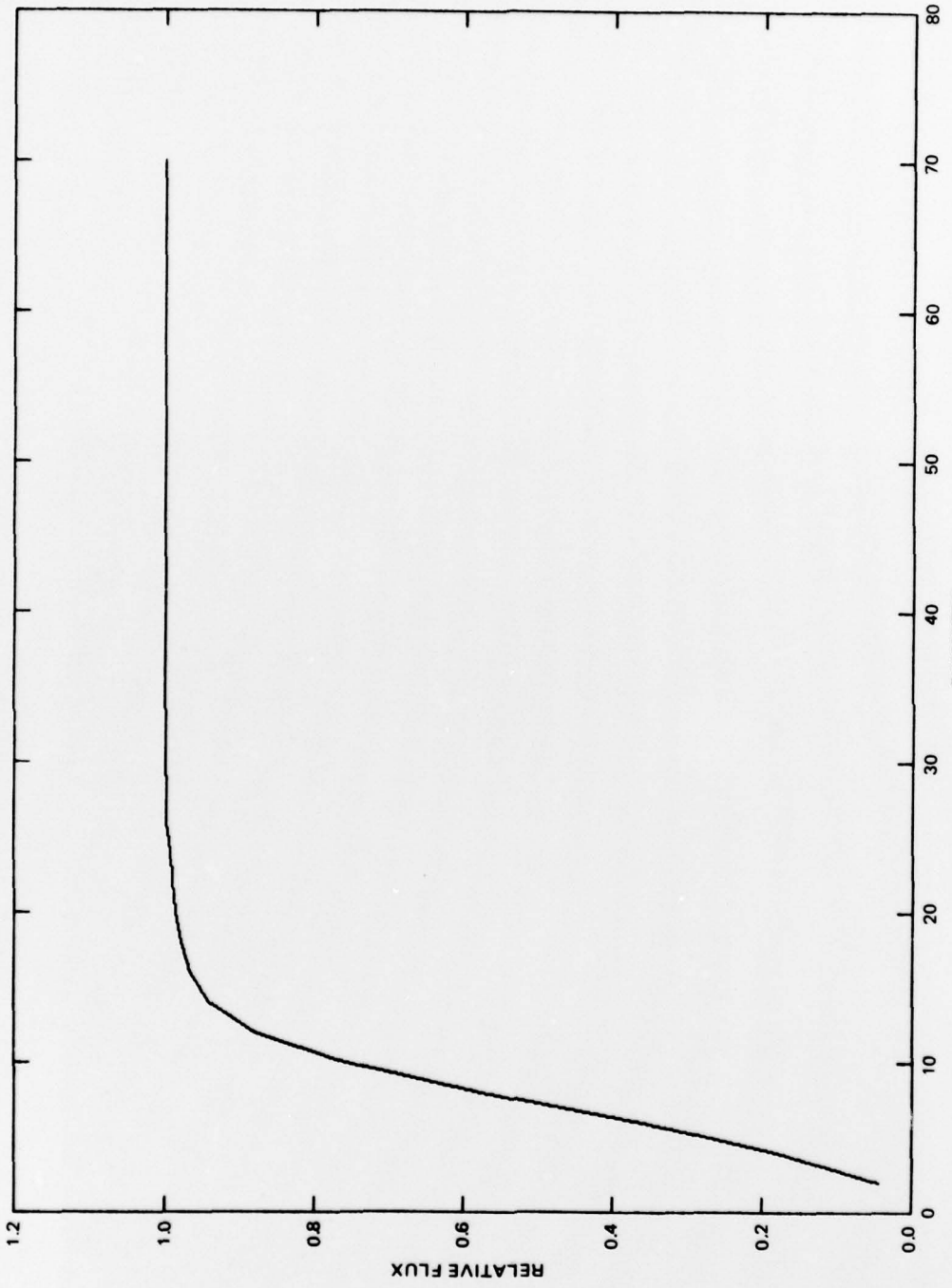

Figure 7(b). DSN119.NF0.

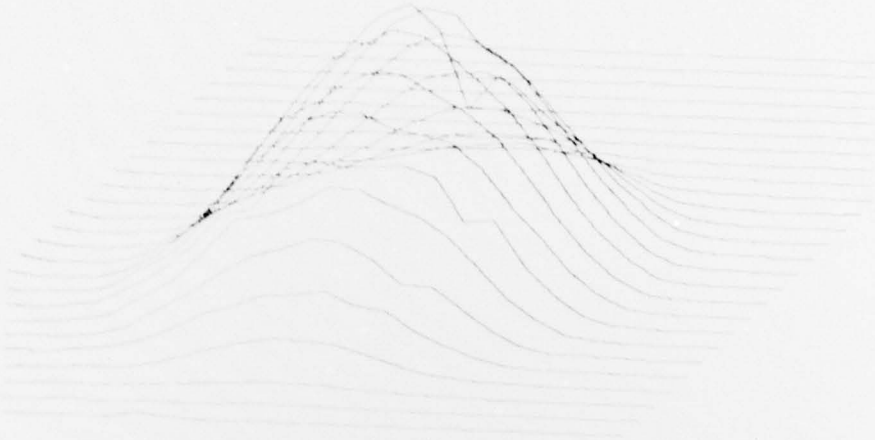

Figure 5(c). DSN120 NF0.

Figure 6(c). DSN120 NF0.

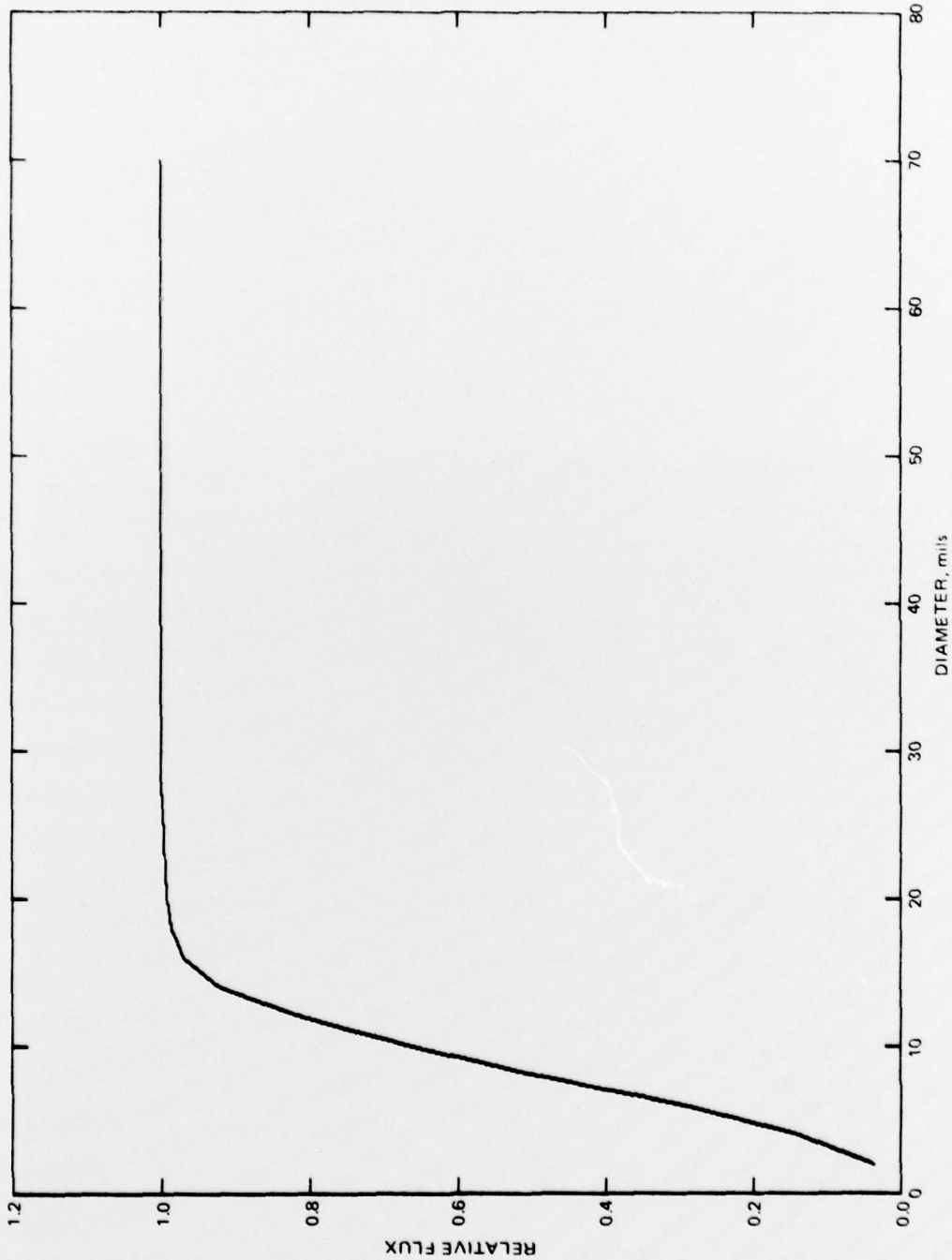

Figure 7(c). DSN120.NF0.

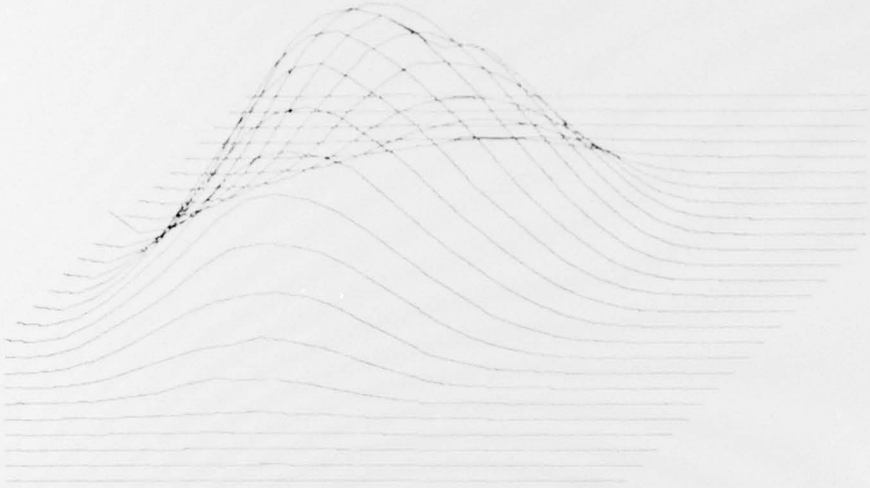

Figure 5(d). DSN121.NF0.

Figure 6(d). DSN121.NF0.

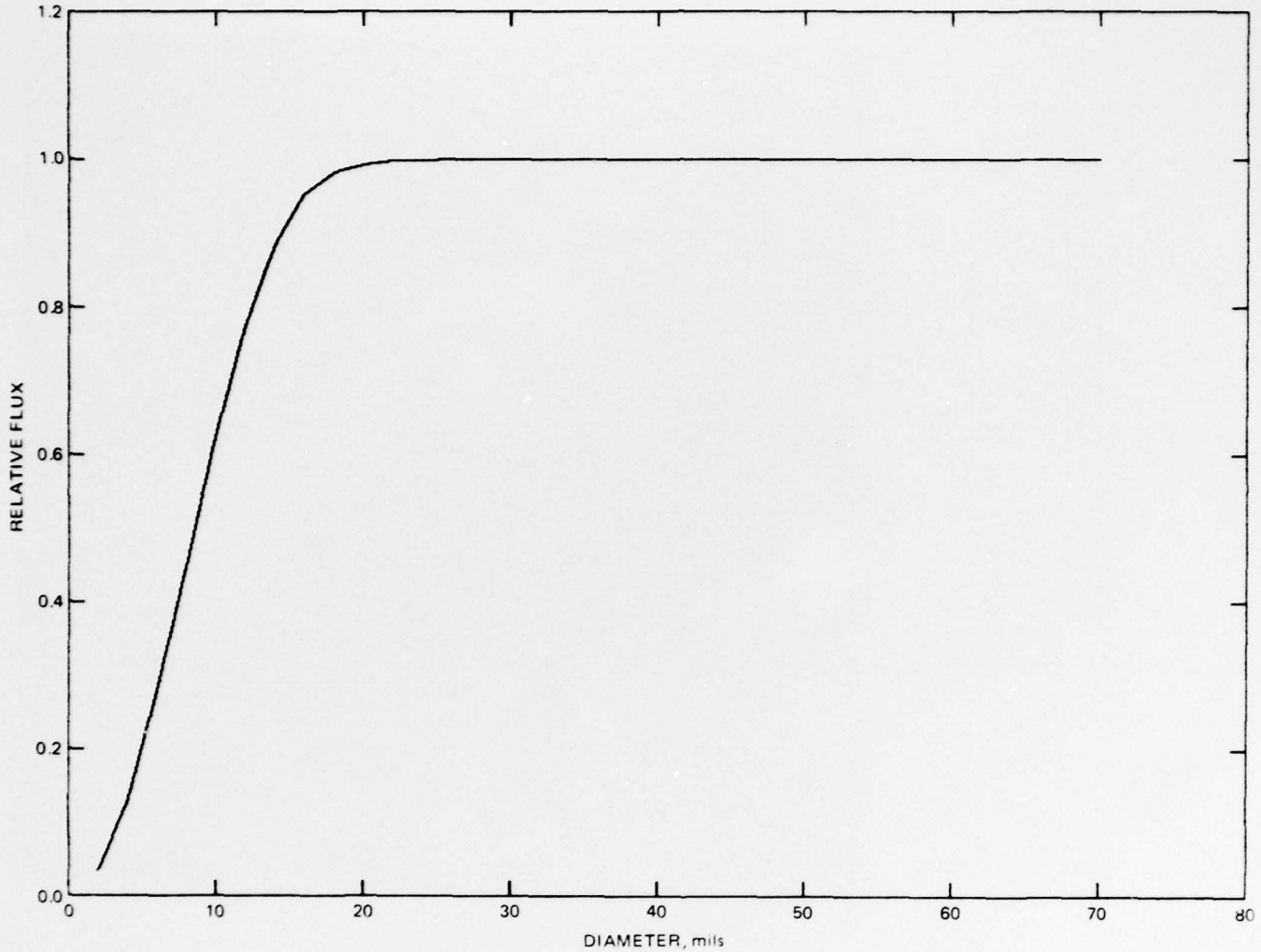

Figure 7(d). DSN121.NF0.

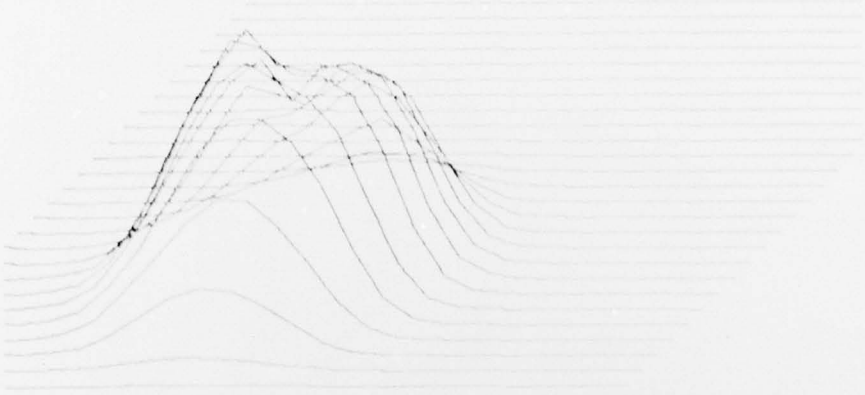

Figure 5(e). DSN122.NE0.

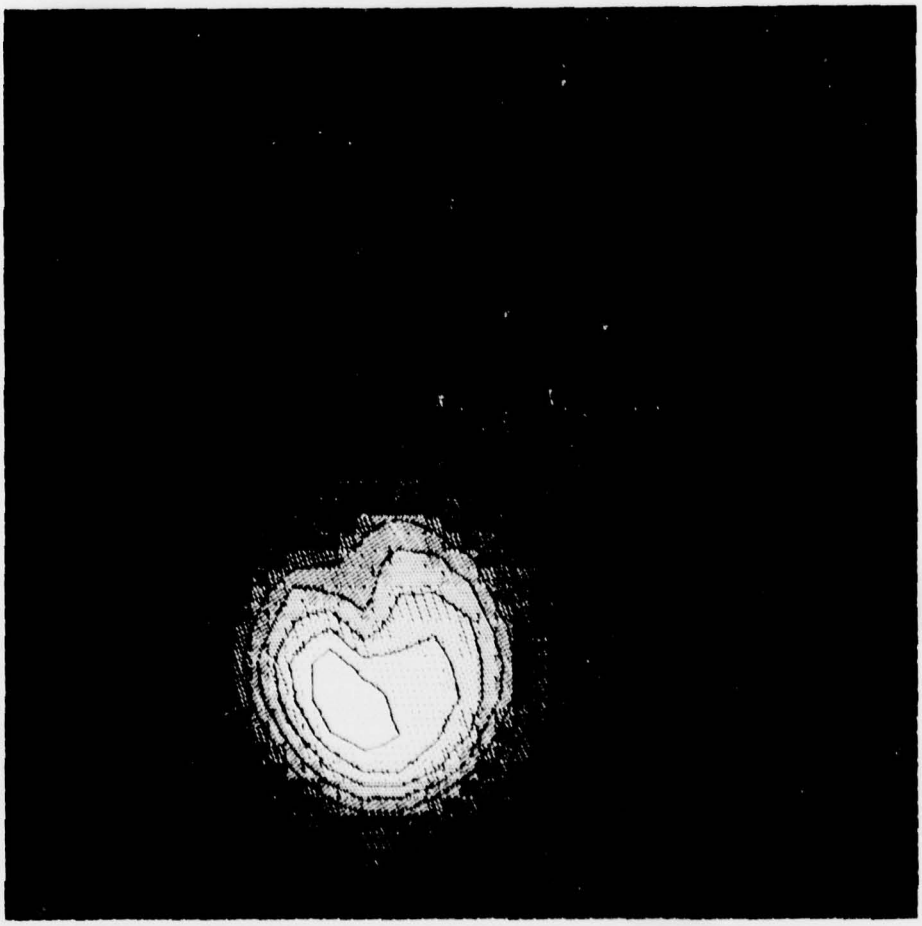

Figure 6(e). DSN122.NE0.

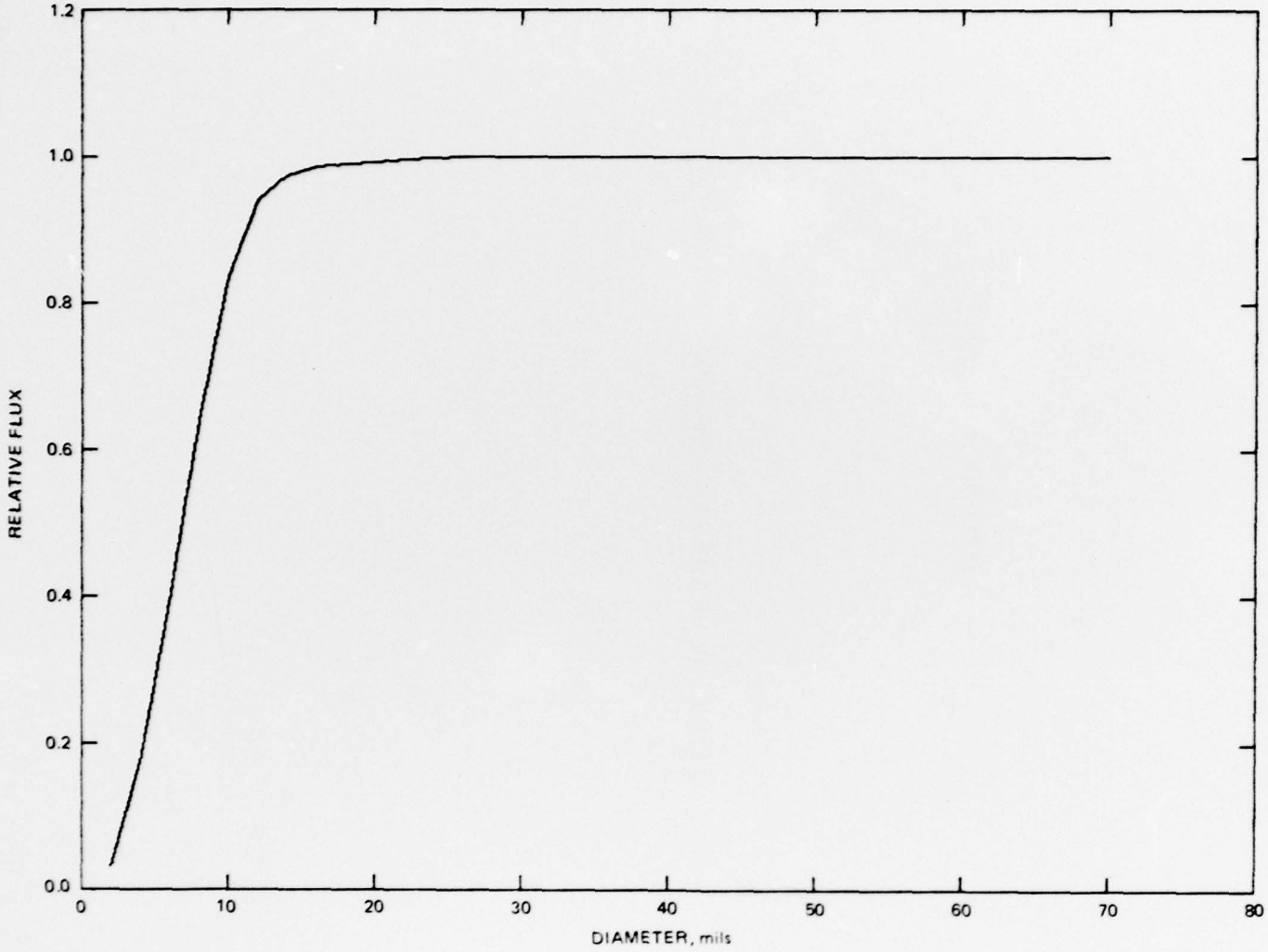

Figure 7(e). DSN122.NF0.

APPENDIX A

GEOMETRY OF THE FAR-FIELD GONIOMETER

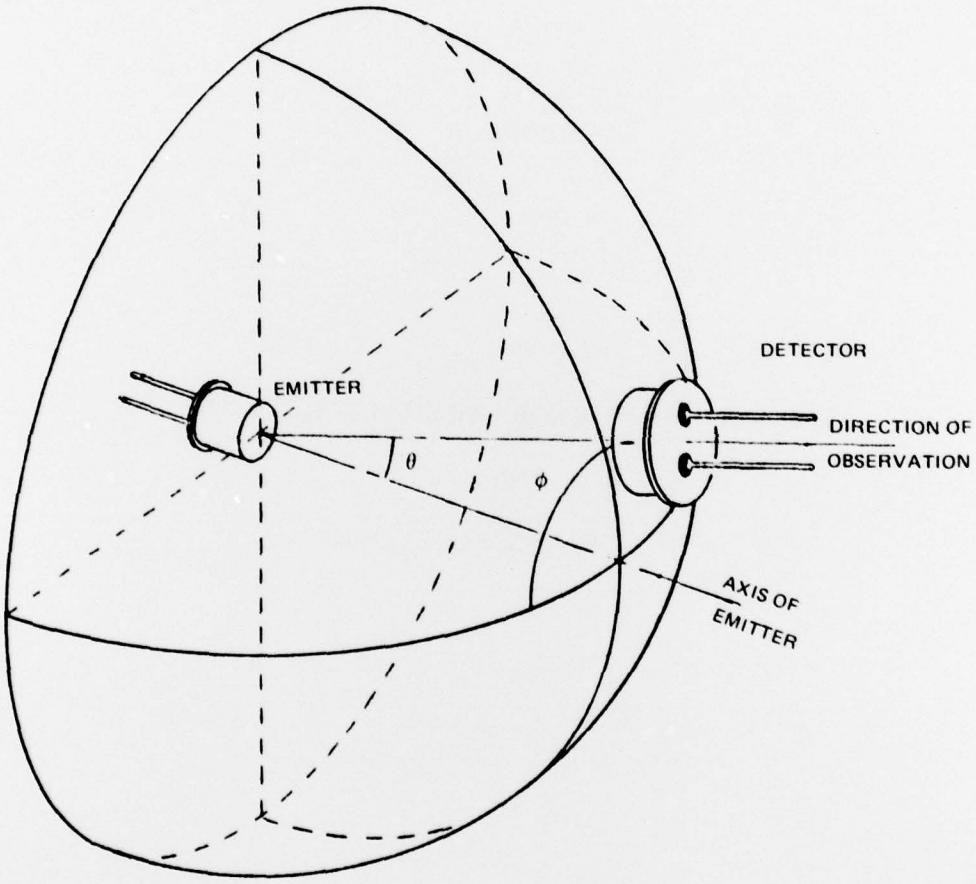

Figure A-1. Geometry of the far-field goniometer.

APPENDIX B

COORDINATE SYSTEM FOR FAR-FIELD GREY SCALE

AND

CONTOUR REPRESENTATIONS

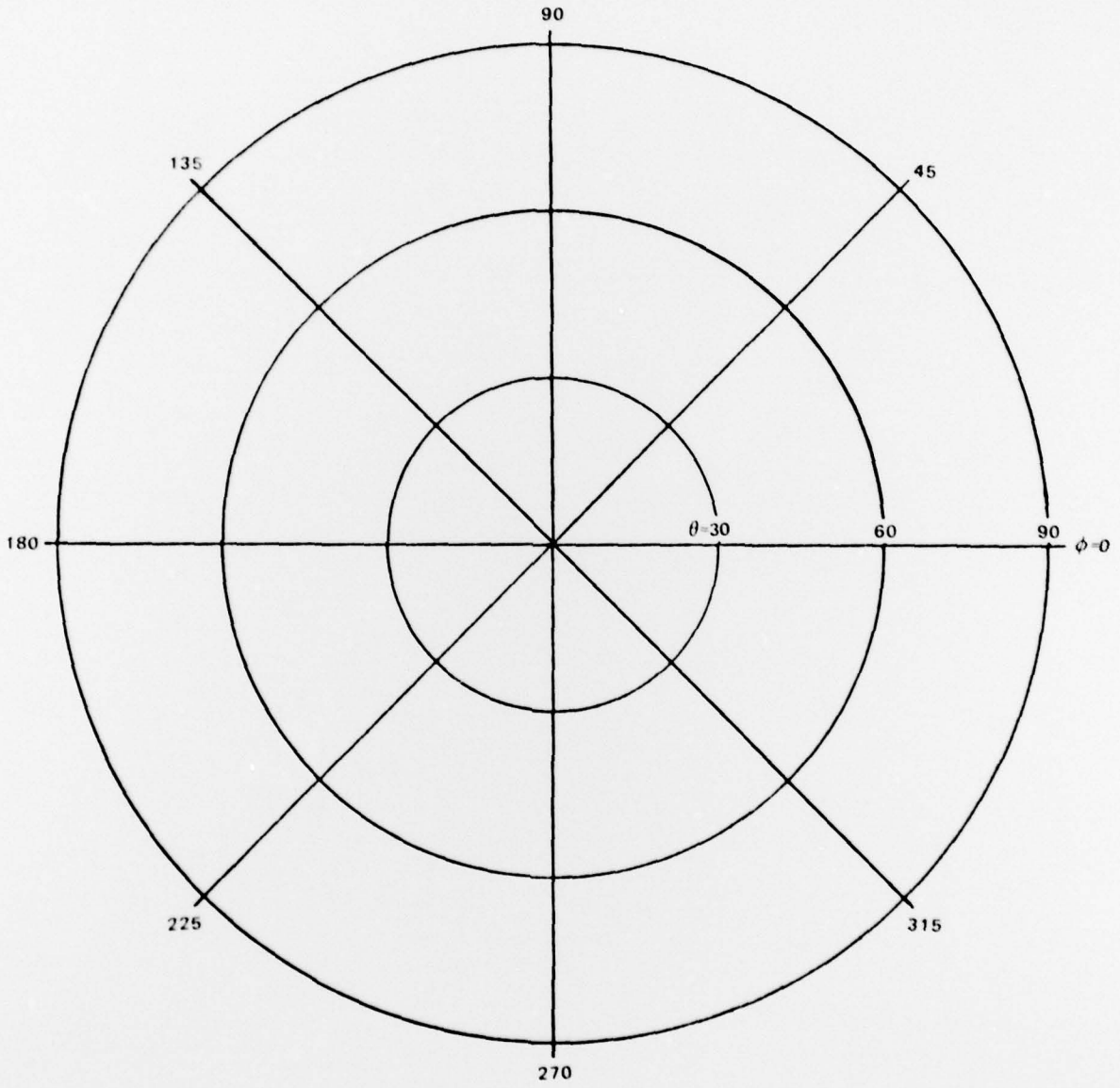

Figure B-1. Coordinate system for far-field grey scale and contour representations.

INITIAL DISTRIBUTION LIST

Antypas, George
Varian Assoc.
611 Hansen Way
Palo Alto, CA 94303

Bahan, Maurice
DRDMI-QS
U. S. Army Missile R&D Comm.
Redstone Arsenal, Alabama 35809

Biard, Dr. Robert
Spectronics, Inc.
830 Arapahoe Road
Richardson, Texas 75080

Buser, Dr. Rudolf
U. S. Army Electronics Command
DRSEL-CT
Ft. Monmouth, N.J. 07703

Casey, Dr. Craig
Room 1C-350
Bell Telephone Laboratories
Murray Hill, N.J. 07974

Coryell, Louis A.
DRDCO-COM-Rm 1
U. S. Army CORADCOM
Ft. Monmouth, N.J. 07703

DAPKUS, P. D. (Dr.)
Electronics Research Division
Autonetics Group
Rockwell International
3370 Miraloma Ave.
P.O. Box 3105
Anaheim, CA 92803

Davies, Eirug
RADC
Hanscom AFB, MA 01731

Day, Gordon
E. M. Division
National Bureau of Standards
Boulder, CO 80302

Dierschke, Dr. Eugene G.
Advanced Opto Technology
Texas Instruments, Inc.
P.O. Box 5012 (M.S. 34)
Dallas, Texas 75222

Dimmock, Dr. John O.
Office of Naval Research
800 N. Quincy St.
Arlington, VA 22217

Foyt, A. George
MIT Lincoln Lab.
Lexington, MA 02173

Franzen, Doug
National Bureau of Standards
Boulder, CO. 80302

Giallorenzi, Thomas
Naval Research Laboratory
Washington, D.C. 20375

Gill, Robert B.
Laser Diode Laboratories,Inc.
205 Forrest Street
Metuchen, N.J. 08840

Glista, Andrew
Code 52022-G
Naval Air Systems Command
Washington, D.C. 20361

Gove, Ron
National Security Agency
Ft. George Meade, Md.20755

Hansen, Del
Hewlett-Packard Laboratories
1501 Page Mill Rd.
Palo Alto, Ca. 94304

Hutcheson, Guilford
Commanding General
USA MIRADCOM
Attn: DRDMI-QTR
Redstone Arsenal, Alabama 35809

Katz, Rod
Code 8B
NAFI-Naval Avionics Center
600 E. 21st St.
Indianapolis, Ind. 46218

Kressel, Henry
RCA Laboratories
David Sarnoff Research Center
Princeton, N.J. 08540

Loskoe, Claire
Amsel-KL-SM
USAECOM, Electr. Comp. Lab.
Ft. Monmouth, N.J. 07703

Mc Sperron, Donald
B308, Metrology Building
National Bureau of Standards
Washington, D.C. 20234

Phelan, Robert
National Bureau of Standards
Boulder, CO 80302

Rosati, Vincent
U.S. Army Electronics Command
DRSEL-CT-LD
Ft. Monmouth, N. J. 07703

Siegman, Dr. Martin
NAVMAT 08T243
Nav. H.Q. CP5, Room 1044
Washington, D.C. 20360

Smith, Byron
Western Regional Standards Lab.
North Island Naval Air Station
San Diego, Ca. 92135

Smith, R.G.
Photodetectors and Receiver Subsystems
Bell Laboratories
Murray Hill, New Jersey 07974

Tomasetta, L.
Rockwell International Science Center
1049 Camino Dos Rios
Thousand Oaks, CA 91360

Trumble, Ken
AFAL/AAD
Air Force Avionics Lab.
Wright Patterson AFB, Ohio 45433

Wilkins, George A.
Naval Undersea Center P.O. Box 997
Kailua, Hawaii 96734

Willis, James
Code AIR-310B
Naval Air Systems Command
Washington, D.C. 20361

Yang, Andrew
RADC/ESO, Stop 30
Hanscom A.F.B., Mass. 01731

Zalewski, Ed. F.
National Bureau of Standards
Gaithersburg, Md. 20760

Dr. Howard Wichanski
US Army Communications Research &
Development Command
ATTN: DRDCO-COM-RN-1
Fort Monmouth, N.J. 07703

Mr. Arnold Flores
Naval Ocean Systems Center
ATTN: Code 9242
San Diego, CA 92152

Air Force Materials Laboratory
ATTN: AFML/LTE
Wright-Patterson AFB, Ohio 45433

Dr. Steven Miller, Chairman
Naval Ocean Systems Center
ATTN: Code 9223
San Diego, CA 92152

Dr. Stanley Kronenberg
US Army Research & Development Command
ATTN: AMSEL-TL-EN
Ft. Monmouth, N.J. 07703

Mr. K.R. Hutchinson
Air Force Avionics Laboratory
ATTN: AFAL/DHO-2
Wright-Patterson AFB, Ohio 45433

Mr. Stewart Share (alternate)
Harry Diamond Laboratory
ATTN: 2800 Powder Mill Road
Adelphi, Maryland 20783

Mr. D. N. Williams, Chairman
Naval Ocean Systems Center
ATTN: Code 825
San Diego, CA 92152

Dr. George Sigel
Naval Research Laboratory
ATTN: Code 6440
Washington, D.C. 20375

CAPT Robert Dunn
Air Force Weapons Laboratory
ATTN: AFWL/ELP
Kirkland AFB, New Mexico 87117

Dr. L. Dworkin
US Army Communications Research
and Development Command
DRDCO-COM-RM1
Ft. Monmouth, NJ 07703

Mr. Nathan Butler
Naval Electronics Systems Command
ATTN: Code NAVELEX 304
Washington D.C. 20361

Mr. Martin Wapner
Naval Sea Systems Command
ATTN: NAVSEA 034
Washington, D.C. 20360

Mr. Dave Anderson
HQ Air Force Systems Command
ATTN: AFSC/DLCAA
Andrews AFB, MD 20334

CDR William E. Hodkins
Office of Naval Research
ATTN: Code 411
Arlington, Va 22217

MAJ Harry Winsor
Materials Science Office
Defense Advanced Research Projects Agency
1400 Wilson Blvd.
Arlington, VA 22209

Mr. A.L. Izzo
Defense Communications Agency
ATTN: Code R320
1860 Wiehle Ave.
Reston, VA 22090

Mr. Alexander Mondrick
US Army Communications Research &
Development Command
ATTN: DRDCO-COM-RM-1
Ft. Monmouth, NJ 07703

Defense Documentation Center (12)

Mr. Robert Lebduska
Naval Ocean Systems Center
ATTN: Code 9242
San Diego, CA 92152

Mr. T. Dellecave (alternate)
Rome Air Development Center
ATTN: RADC/RBRM
Griffiss AFB, New York 13441

Mr. D.A. Zann
Air Force Avionics Laboratory
ATTN: AFAL/AAT
Wright-Patterson AFB, Ohio 45433

Mr. R.M. Christian (alternate)
US Army Communications Research &
Development Command
ATTN: DRDCO-COM-RM-4
Ft. Monmouth, NJ 07703

Mr. D.N. Williams
Naval Ocean Systems Center
ATTN: Code 825
San Diego, CA 92152

Mr. D. Howard (alternate)
Naval Electronic Systems Security
Engineering Center
ATTN: Code 02
3801 Nebraska Ave., N.W.
Washington, D.C. 20390

Dr. Richard Payne
Air Force Rome Air Development Center
ATTN: RADC/ESO
Hanscom AFB
Bedford, Mass. 01731

CAPT J. Huertas
ESD/MCES
Hanscom AFB
Bedford, Mass. 01731

Mr. Boyd C. Wooton, Chairman
National Security Agency
ATTN: R-13
Fort George G. Meade, MD 20755